

Dinuclear helicate and tetranuclear cage assembly using appropriately designed ditopic triazole-azine ligands

Sandhya Singh, Ross W. Hogue, Humphrey L. C. Feltham and Sally Brooker*

Department of Chemistry and the MacDiarmid Institute for Advanced Materials and Nanotechnology, University of Otago, PO Box 56, Dunedin 9054, New Zealand

Electronic Supplementary Information

X-ray Crystallography

L^{4pym-meta}: All hydrogen atoms were placed in calculated positions and rode on the attached carbon atom with $U(H)=1.2U(X)$. All non-H atoms were refined anisotropically. No disorder is present. For further details see Table S8, Figure S42 and the cif file.

L^{2pym-para}: All hydrogen atoms were placed in calculated positions and rode on the attached carbon atom with $U(H)=1.2U(X)$. All non-H atoms were refined anisotropically. No disorder is present. For further details see Table S8, Figure S43 and the cif file.

[Fe₂(L^{2pym-meta})₃](BF₄)₄·6CH₃CN (1·6CH₃CN): All hydrogen atoms were placed in calculated positions and rode on the attached carbon atom with $U(H)=1.2U(X)$. All non-H atoms were refined anisotropically. C10 and C9 (bridging phenylene linker) have larger thermal ellipsoids but this is best modelled this way. For further details see the cif file.

[Fe₂(L^{4pym-meta})₃](BF₄)₄·6CH₃CN (2·6CH₃CN): All hydrogen atoms were placed in calculated positions and rode on the attached carbon atom with $U(H)=1.2U(\text{attached atom, C})$. All non-H atoms were refined anisotropically. Carbon atoms (and associated H atoms) of one isobutyl group were disordered across two positions with occupancy 0.333 (C7A, C8A and C9A) and 0.667 (C7B, C8B and C9B).

[Fe₄(L^{2pym-para})₆](BF₄)₈ (3·solvent): All hydrogen atoms were placed in calculated positions and rode on the attached carbon atom with $U(H)=1.2U(\text{attached atom, C})$. All non-H atoms were refined anisotropically. Out of three isobutyl groups two were disordered. The disorder was modelled for one of them, constrained by $RIGU\ C32 > C35$ (0.6 occupancy C33B and C34B; 0.4 occupancy C33C and C34C), along with the affected H atoms (including on full occupancy C32 and C35). The second one which showed signs of disorder (C20, C21, C22), could not be modelled satisfactorily so was left with higher thermal ellipsoids. All of the solvent molecules of crystallisation were highly disordered and could not be modelled well so SQUEEZE¹ was applied in PLATON.² The electron density found by SQUEEZE was 2749 electrons/cell i.e. 344 electrons per cage ($Z=8$). This is in agreement with the presence of approximately 10 molecules of nitromethane ($10 \times 32 = 320$ electrons) per cage.

[Fe₄(L^{4pym-para})₆](BF₄)₈ (4·solvent): All hydrogen atoms were placed in calculated positions and rode on the attached carbon atom with $U(H)=1.2U(\text{attached atom})$. All non-H atoms were refined anisotropically. All of the solvent molecules of crystallisation and seven of the eight BF₄⁻ counter-anions were highly disordered and could not be modelled well so SQUEEZE¹ was applied in PLATON.² The electron density found by SQUEEZE was 2166 electrons/cell i.e. 541 electrons per complex ($Z=4$). This is in agreement with the presence of 7 molecules of BF₄⁻ ($7 \times 41 = 287$ electrons) and approximately 11 molecules of acetonitrile ($11 \times 22 = 242$ electrons) per cage; a total of 529 electrons.

High resolution pictures were prepared using Mercury³ and POVray⁴ software. Details of the data collections and refinements are given in Tables S1 and S8. Crystallographic data for the structures have been deposited with the Cambridge Crystallographic Data Centre, CCDC 1913951-1913956.

Table S1. Crystal Data and Structure Refinement Details for the complexes.

	1·6CH ₃ CN	2·6CH ₃ CN	3· solvent	4· solvent
Empirical formula	C ₉₀ H ₁₀₂ B ₄ F ₁₆ Fe ₂ N ₃₆	C ₉₀ H ₁₀₂ B ₄ F ₁₆ Fe ₂ N ₃₆	C ₁₅₆ H ₁₆₈ B ₈ F ₃₂ Fe ₄ N ₆₀	C ₁₅₆ H ₁₆₈ BF ₄ F ₄ e ₄ N ₆₀
M _r	2146.97	2146.97	3801.37	3193.70
Crystal system	Trigonal	Trigonal	orthorhombic	monoclinic
Space group	P-31c	P-31c	Fddd	P2 ₁ /n
a [Å]	13.9828(4)	14.0744(5)	24.4140(10)	18.8183(4)
b [Å]	13.9828(4)	14.0744(5)	40.903(3)	35.8024(8)
c [Å]	29.5355(9)	28.3720(10)	42.307(5)	31.8118(6)
α [°]	90	90	90	90
β [°]	90	90	90	105.862(2)
γ [°]	120	120	90	90
V [Å ³]	5001.1(3)	4867.2(4)	42248(6)	20616.8(8)
Z	2	2	8	4
T [K]	100	100	100	100
ρ _{calcd.} [g/cm ³]	1.426	1.465	1.195	1.029
μ [mm ⁻¹]	3.140	3.226	2.893	2.688
F(000)	2220.0	2220.0	15648.0	6676.0
Crystal Size (mm)	0.3 × 0.2 × 0.1	0.9 × 0.7 × 0.6	0.1 × 0.05 × 0.02	0.2 × 0.08 × 0.05
2θ range for data collection (Cu radiation)	7.3 to 150.03°	7.252 to 153.704°	7.556 to 153.314	6.944 to 153.57°
Reflections collected	17009	13619	41452	97215
Independent reflections	3408	3397	10954	42259
R(int)	0.0273	0.0426	0.0894	0.0692
Data / restraints / parameters	3408/0/227	3397/3/264	10954/33/612	42259/0/2050
Goof (F ²)	1.054	1.098	1.044	0.985
R ₁ [I>2σ(I)]	0.0518	0.0688	0.0969	0.0749
wR ₂ [all data]	0.1431	0.2084	0.2999	0.2189
Max/min res. e density [eÅ ⁻³]	0.97 and -0.42	1.42 and -1.59	1.52 and -0.78	0.98 and -0.57

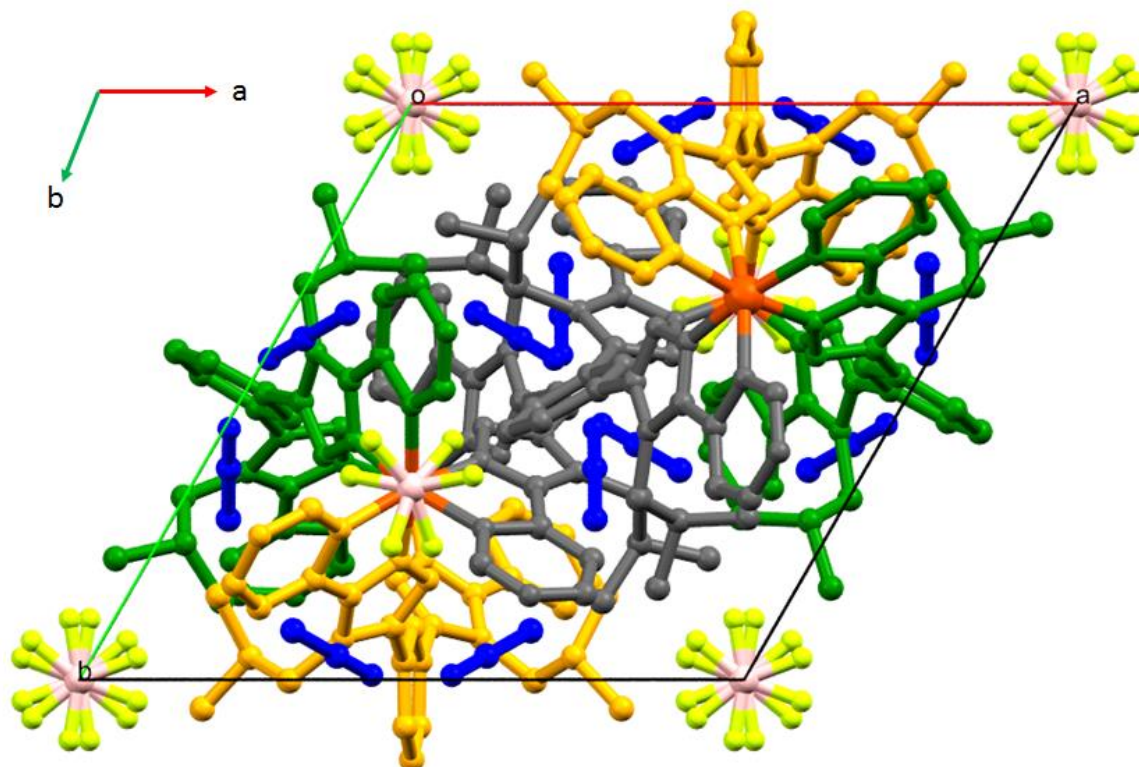


Figure S1. Representation of the unit cell contents for $[\text{Fe}_2(\text{L}^{2\text{pym-meta}})_3](\text{BF}_4)_4 \cdot 6\text{MeCN}$ (**1**), viewed down the *c*-axis ($Z=2$). The isomorphous helicate $[\text{Fe}_2(\text{L}^{4\text{pym-meta}})_3](\text{BF}_4)_4 \cdot 6\text{MeCN}$ (**2**), has the same packing arrangement. The helical strands lie along the *c*-direction, wrapping around the pairs of iron centres. Solvent molecules (blue). For each complex the three ligand strands are in three different colours; orange, grey and green. Hydrogen atoms are not shown.

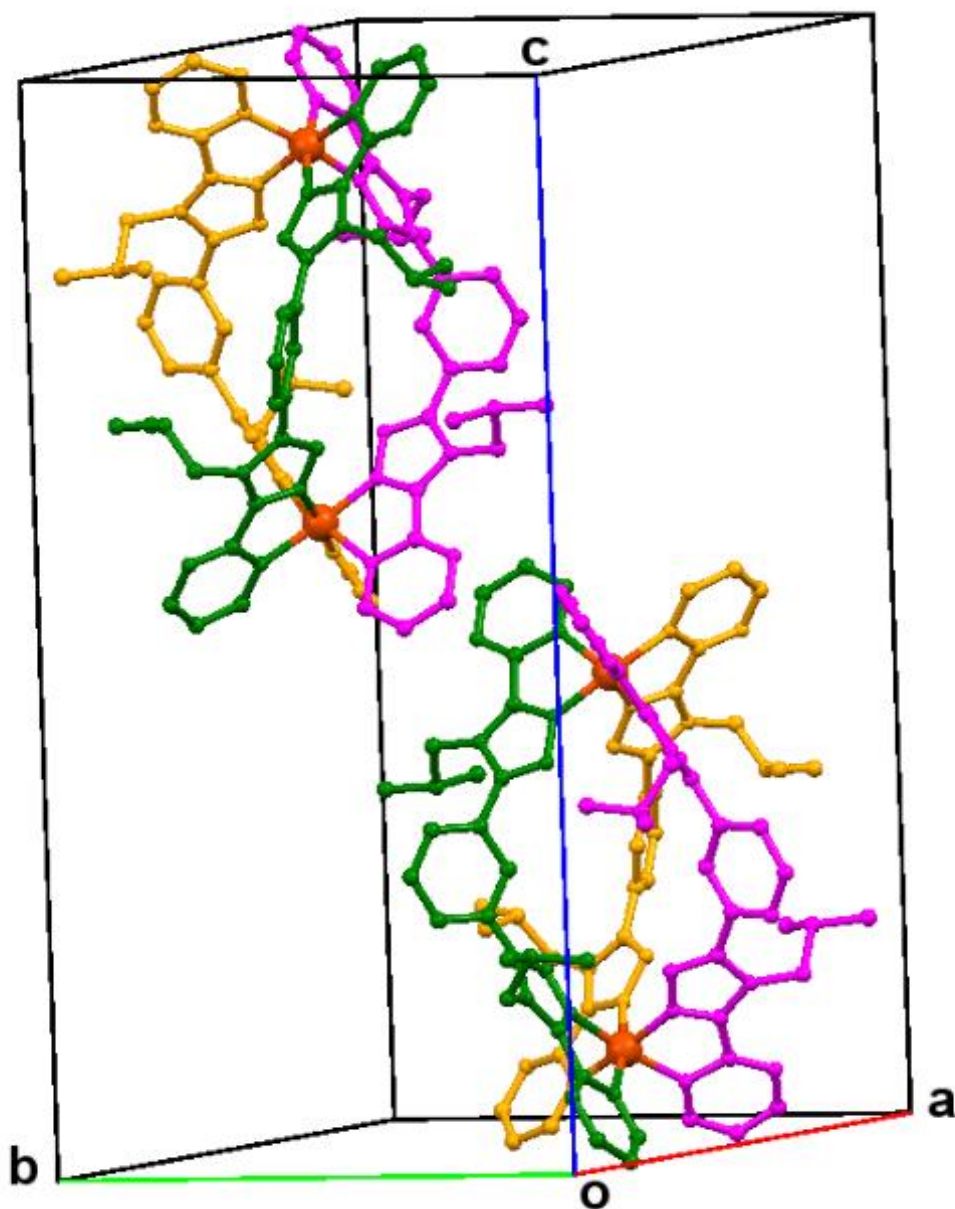


Figure S2. The two homochiral at metal centre ($\Lambda\Lambda$) and ($\Delta\Delta$) isomers present, 1:1, in the unit cell for both helicites **1** and **2** (**1** shown here; but **2** is isostructural).

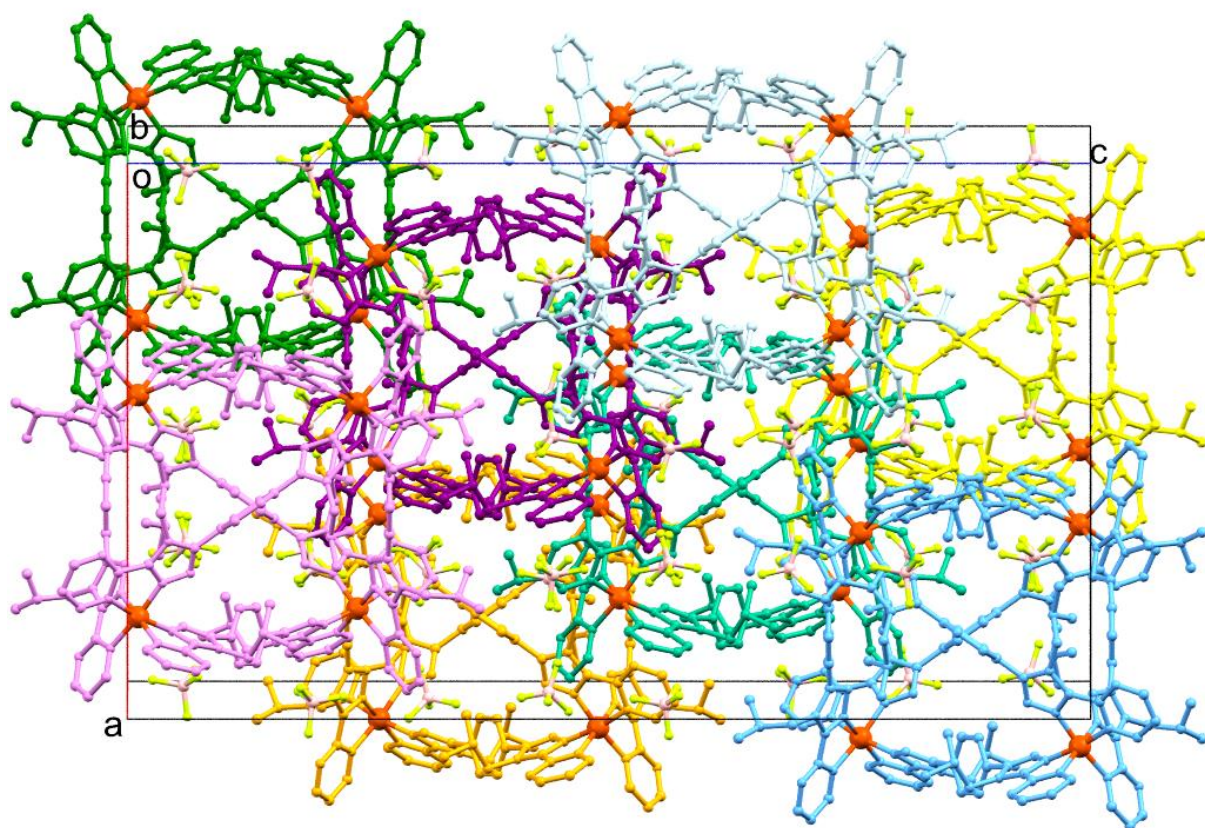


Figure S3. Representation of the unit cell of $[\text{Fe}_4(\text{L}^{2\text{pym-meta}})_6](\text{BF}_4)_8 \cdot \text{xsolvent}$ (**3**), emphasising the alignment of the cages looking down the b-direction ($Z=8$). Each tetrahedral cage is in a different colour; purple, pink, green, light green, grey, blue, orange and yellow. Hydrogens are not shown. Solvents were treated by SQUEEZE so are not shown.

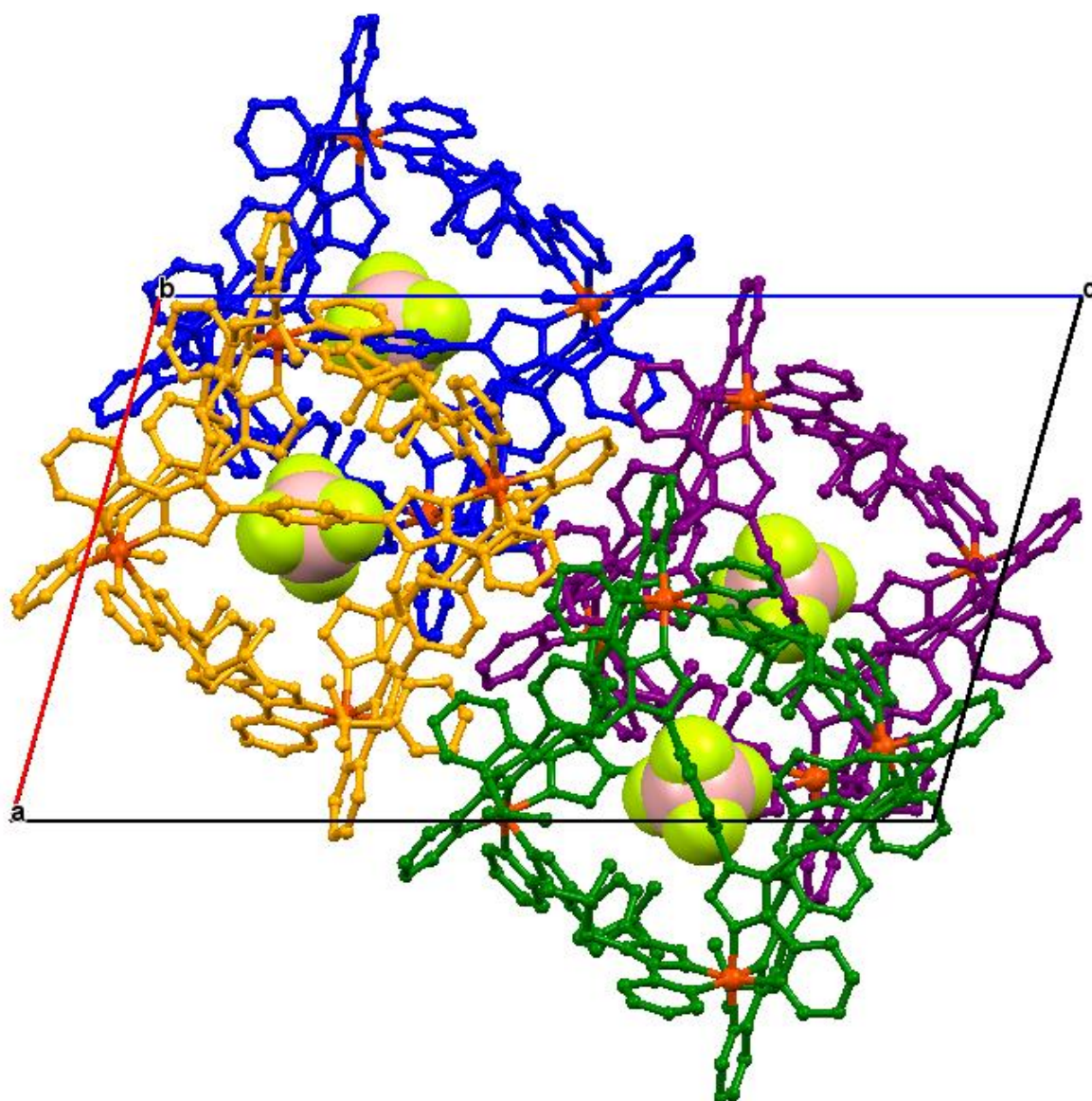


Figure S4. Representation of the lattice of $[\text{Fe}_4(\text{L}^4\text{pym-meta})_6](\text{BF}_4)_8 \cdot \text{solvent}$ (**4**) with encapsulated BF_4 , emphasizing the alignment of cage along b-direction. All tetrahedral cages are in different colours; orange, blue, purple and green. Hydrogens are not shown. Solvents of crystallisation and 7 of the 8 BF_4 were treated by SQUEEZE.

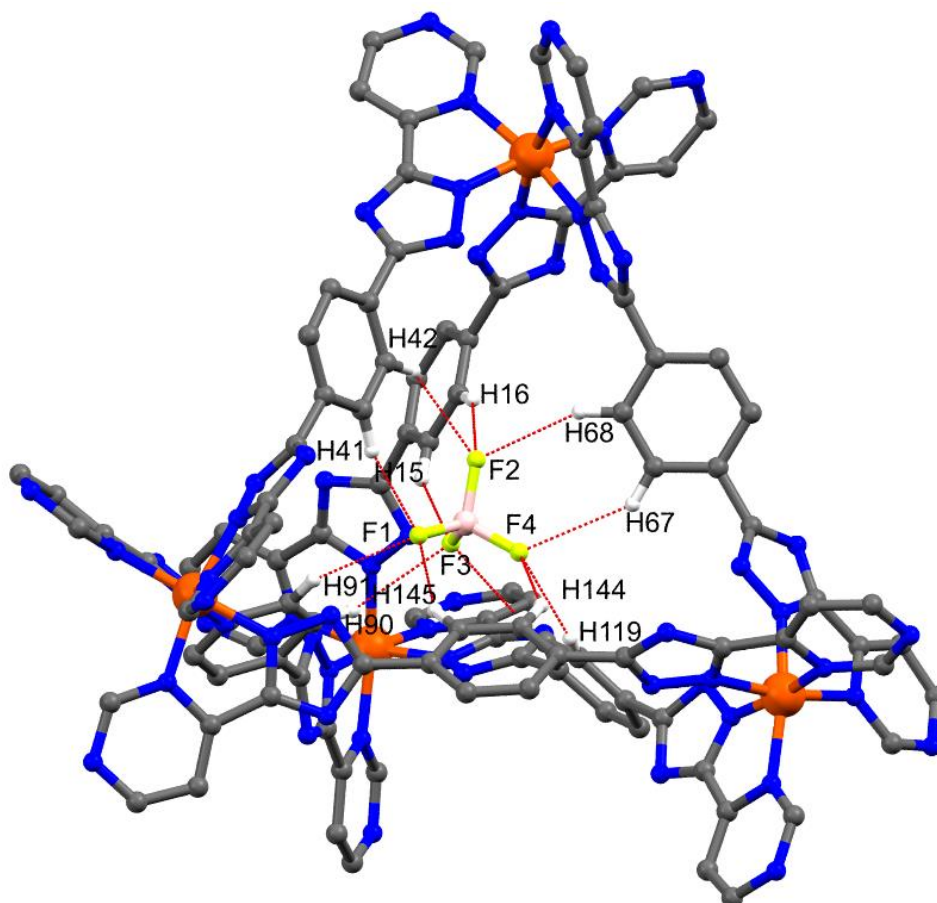


Figure S5. Schematic view of the twelve non-classical C–H...F hydrogen bonds formed between the encapsulated BF_4^- anion and 1,4-phenylene linker in the case of cage **4**.

Table S2. The 12 C–H...F non-classical hydrogen bonds formed between the pairs of internally facing CH moieties of each of the six phenylene spacers and the encapsulated BF_4^- anion in cage **4**.

D–H...A	D–A	H...A Å	Angle D–H...A
C15–H15...F3	3.341	2.537	144.80
C90–H90...F3	3.527	2.738	143.09
C120–H120...F3	3.392	2.578	146.43
C16–H16...F2	3.381	2.536	151.19
C42–H42...F2	3.407	2.620	142.75
C68–H68...F2	3.489	2.660	148.83
C41–H41...F1	3.441	2.585	153.36
C91–H91...F1	3.519	2.664	153.08
C145–H145...F1	3.365	2.505	153.95
C67–H67...F4	3.510	2.722	143.00
C119–H119...F4	3.422	2.585	149.89
C144–H144...F4	3.329	2.539	142.90

Table S3. Pyrimidine-triazole and triazole Fe-phenyl ring angle in **3**. Red angle corresponds to phenylene linker with different conformation from that in **4** (see Fig S6); note that this cage is high symmetry (Fddd) so there is only one such angle.

3			
Pyrimidine-triazole angle	(°)	Triazole Fe-phenyl ring angle	(°)
L C4 N1 C1 C2 C3 N2- N5 C5 N3 N4 C10	3.57	C31 N3 N4 C10 N5 C5 Fe1- C13 C13 C11 C12 C12 C11	79.18
L C17 N7 C16 C15 C14 N6- N10 C18 N8 N9 C23	4.22	C18 N10 C23 N9 N8 Fe1- C24 C26 C25 C24 C26 C25	40.41
L C27 N11 C28 C29 N12 C30- C31 N15 C36 N14 N13	1.06	C36 N15 C31 N13 N14 Fe1- C37 C38 C38 C37 C39 C39	52.00

Table S4. Pyrimidine-triazole and triazole Fe-phenyl ring angle in **4**. Red angles correspond to the two crystallographically independent phenylene linkers that have different conformations from that seen in **3**, in order to hydrogen-bond to the encapsulated BF₄ anion (see Fig S6).

4			
Pyrimidine-triazole angle	(°)	Triazole Fe-phenyl ring angle	(°)
Fe1			
N22 C53 N21 C56 C55 C54- N23 C57 N24 C58 N25	4.14	Fe1 N24 C58 N25 C57 N23- C64 C63 C68 C67 C66 C65	70.61
N1 C4 C3 C2 N2 C1- N4 N5 C6 N3 C5	1.04	Fe1 N4 N5 C6 N3 C5- C12 C11 C13 C14 C15 C16	65.14
C29 C28 N12 C27 N11 C30- C31 N15 C36 N14 N13	4.69	Fe1 N13 C31 N15 C36 N14- C37 C38 C39 C40 C41 C42	62.86
Fe2			
N9 C24 N10 C25 C26 C23- C22 N7 C17 N6 N8	5.57	Fe2 N8 C22 N7 C17 N6- C15 C14 C13 C12 C11 C16	56.96
C105 N42 C106 C107 C108 N41- C109 N43 N44 C114 N45	6.39	Fe2 N43 C109 N45 C114 N44- C118 C117 C116 C115 C120 C119	60.54
C79 N31 C82 C81 C80 N32- C83 N33 N34 C88 N35	6.10	Fe2 N33 C83 N35 C88 N34- C89 C90 C91 C92 C93 C94	59.95
Fe3			
C75 C76 C77 N30 C78 N29- C74 N28 C69 N26 N27	5.86	Fe3 N28 N27 C74 C69 N26- C67 C66 C65 C64 C63 C68	53.31
N49 C127 C128 C129 N50 C130- N46 N47 C126 N48 C121	4.85	Fe3 N47 C126 N48 C121 N46- C118 C117 C116 C115 C120 C119	70.03
C133 C132 N52 C131 N51 C134- N54 C140 N55 C135 N53	4.65	Fe3 N53 C135 N55 C140 N54- C141 C142 C143 C146 C145 C144	63.57
Fe4			
N59 C153 C154 C155 N60 C156- N57 C152 N58 C147 N56	4.83	Fe4 N57 C152 N58 C147 N56- C146 C143 C142 C141 C144 C145	62.39
C50 C51 N20 C52 N19 C49- C48 N18 C43 N16 N17	6.66	Fe4 N17 C48 N18 C43 N16- C40 C39 C38 C37 C42 C41	63.98
C102 C103 N40 C104 N39 C101- C100 N38 C95 N36 N37	1.79	Fe4 N37 C100 N38 C95 N36- C92 C93 C94 C89 C90 C91	65.08

Table S5. Fe...Fe distances (Å) and Fe...Fe...Fe angles (°) in cages **3** and **4**.

3		4	
Fe...Fe (Å)	13.442(1)	Fe1...Fe2	13.4048(9)
	13.328(2)	Fe1...Fe3	13.286(1)
	13.152(1)	Fe1...Fe4	13.290(1)
		Fe2...Fe3	13.410(1)
		Fe2...Fe4	13.2731(8)
		Fe3...Fe4	13.3223(9)
Fe...Fe...Fe (°)		Fe2...Fe1...Fe3	60.32
	60.14(1)	Fe2...Fe1...Fe4	59.75
	61.01(1)	Fe3...Fe1...Fe4	60.17
	58.85(1)	Fe1...Fe2...Fe4	59.75
		Fe3...Fe2...Fe4	59.90
		Fe1...Fe2...Fe3	59.40
		Fe1...Fe3...Fe2	60.28
		Fe2...Fe3...Fe4	59.54
		Fe1...Fe3...Fe4	59.93
		Fe1...Fe4...Fe3	59.90
		Fe1...Fe4...Fe2	60.62
		Fe2...Fe4...Fe3	60.56

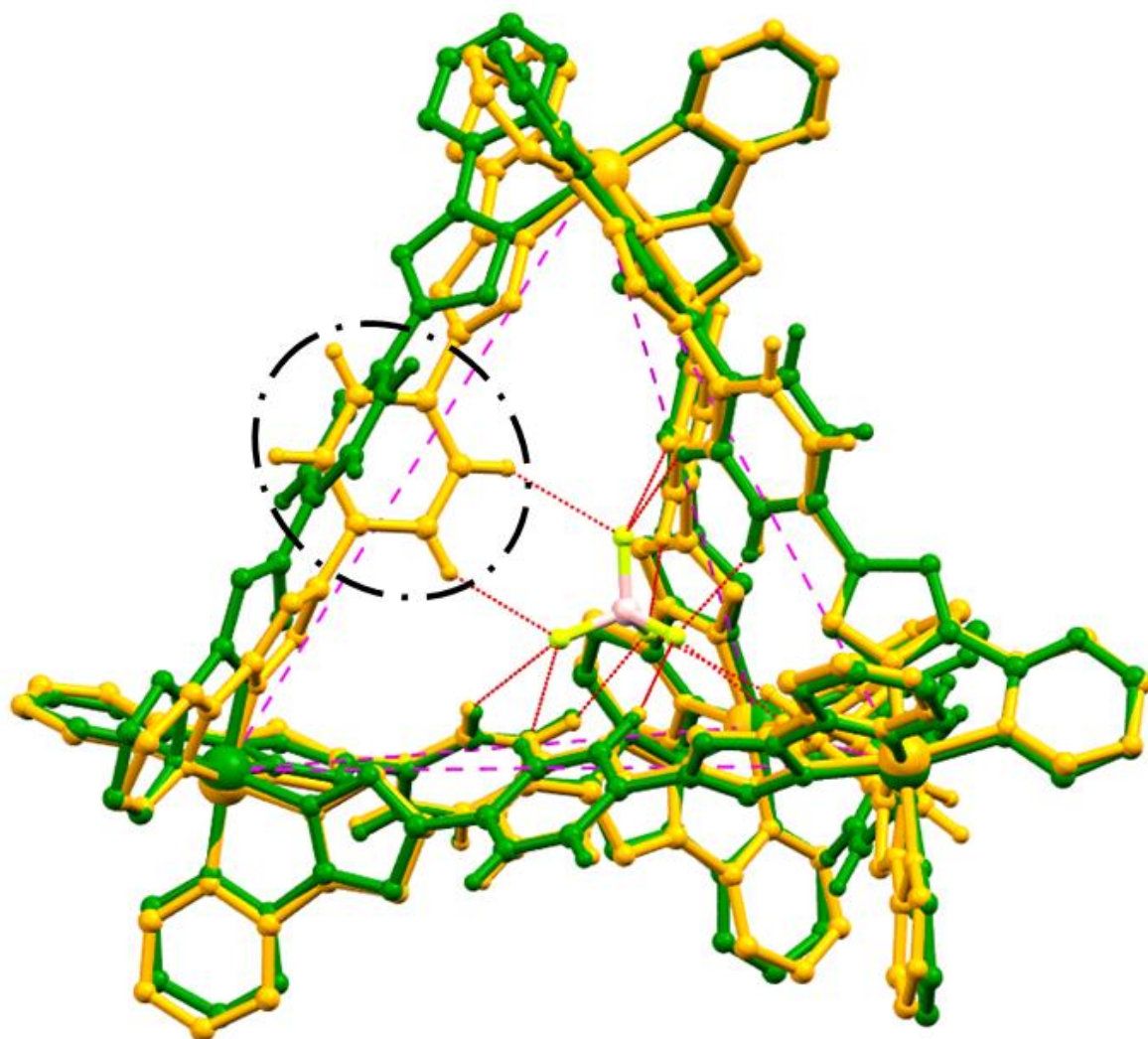


Figure S6. This overlay of the structures of **3** (green) and **4** (yellow) reveals the difference in the angle of one of the phenyl rings forming an edge of the cage which occurs in order to optimise hydrogen bonding to the encapsulated anion in the case of **4**. Hydrogen atoms, except those on the phenylene spacers, and iso-butyl groups are not shown for clarity.

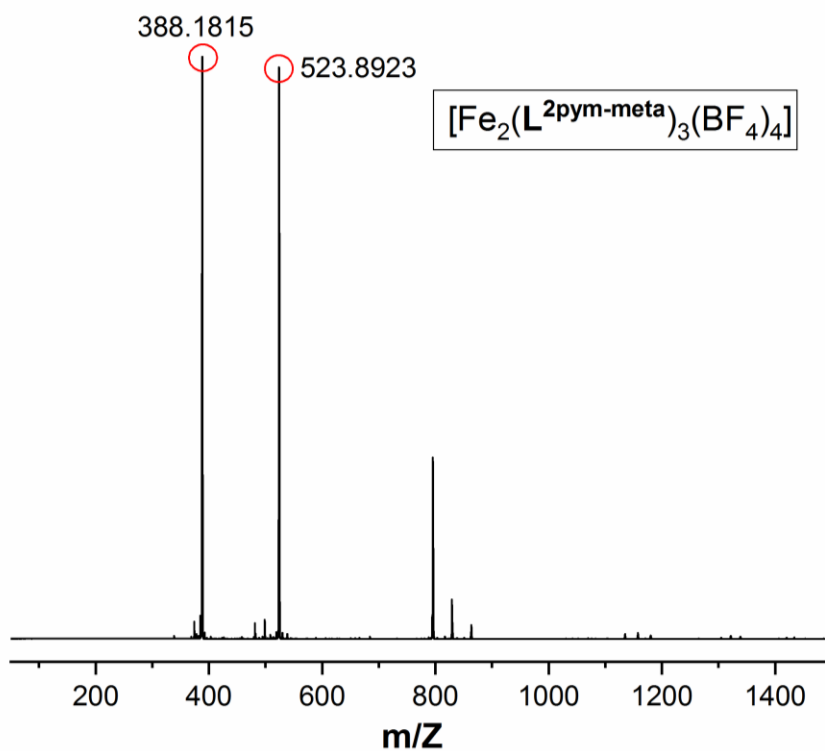


Figure S7. Mass spectrum of $[\text{Fe}_2(\text{L}^{2\text{pym-meta}})_3](\text{BF}_4)_4$ (**1**). Fits of the circled peaks are provided in the following figures.

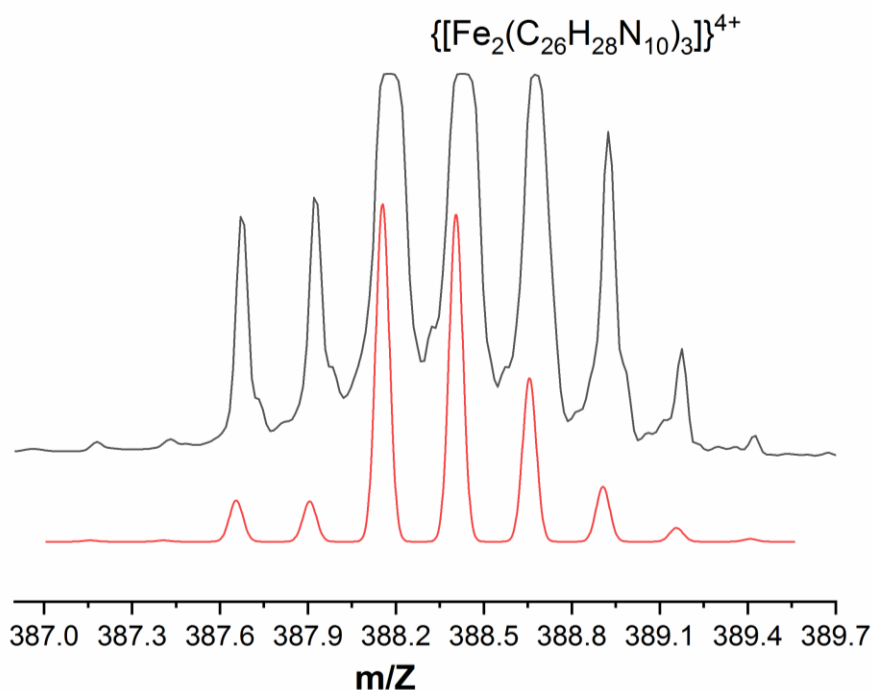


Figure S8. Fit of a peak in the mass spectrum of $[\text{Fe}_2(\text{L}^{2\text{pym-meta}})_3](\text{BF}_4)_4$ (**1**) (Figure S7): $[\text{Fe}_2(\text{L}^{2\text{pym-meta}})_3]^{4+}$ experimental (black) and simulated pattern (red).

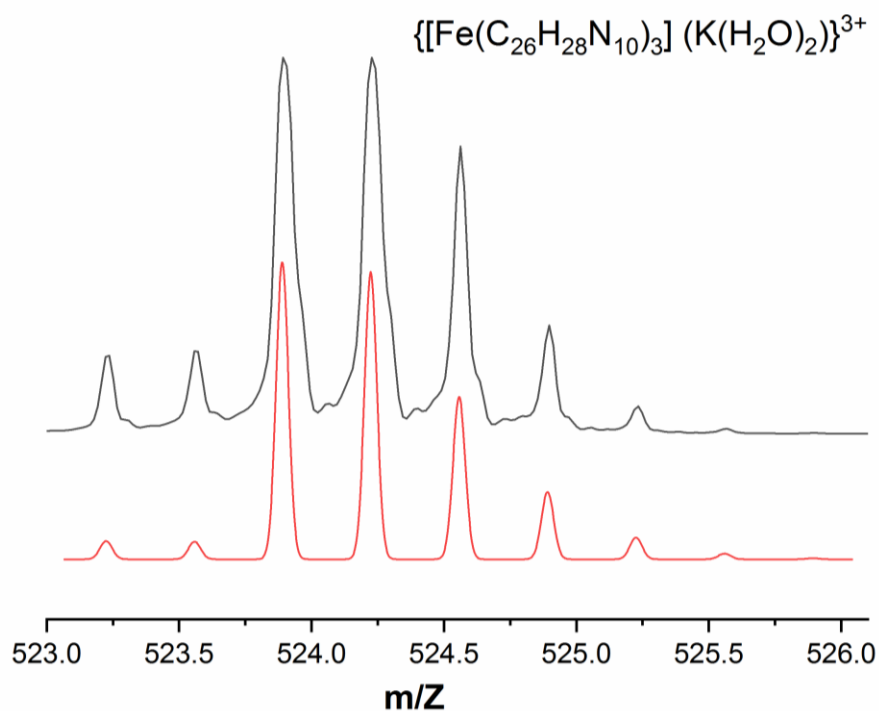


Figure S9. Fit of a peak in the mass spectrum of $[\text{Fe}_2(\text{L}^{2\text{pym-meta}})_3](\text{BF}_4)_4$ (**1**) (Figure S7): $\{[\text{Fe}(\text{L}^{2\text{pym-meta}})_3](\text{K}(\text{H}_2\text{O})_2)\}^{3+}$ experimental (black) and simulated pattern (red).

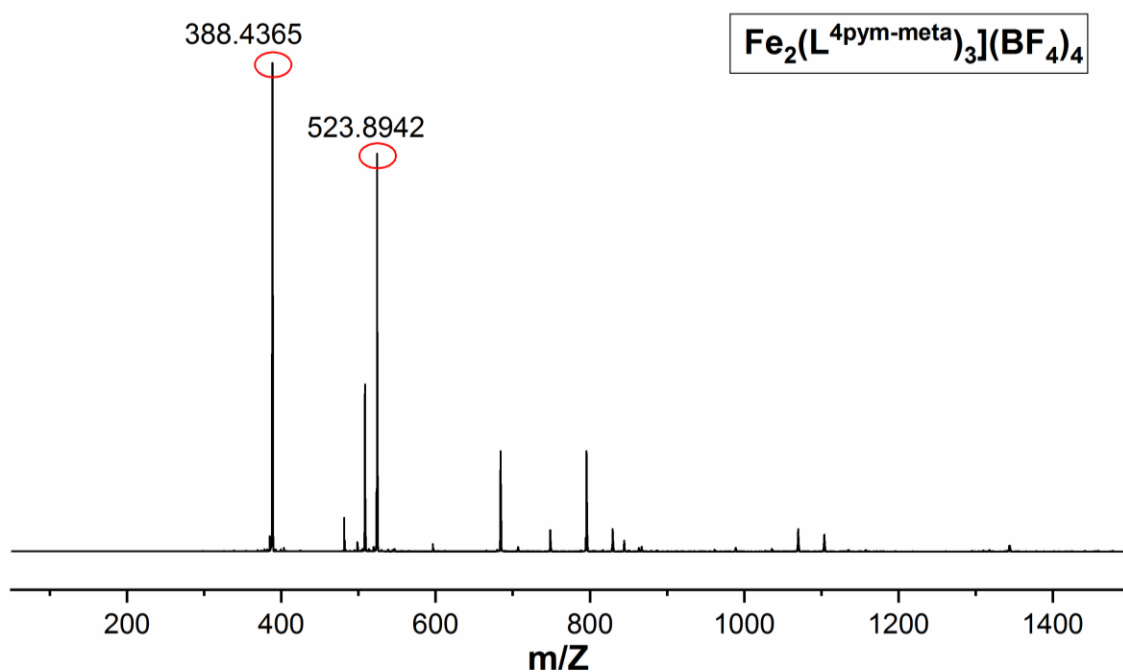


Figure S10. Mass spectrum of $[\text{Fe}_2(\text{L}^{4\text{pym-meta}})_3](\text{BF}_4)_4$ (**2**). Fits of the circled peaks are provided in the following figures.

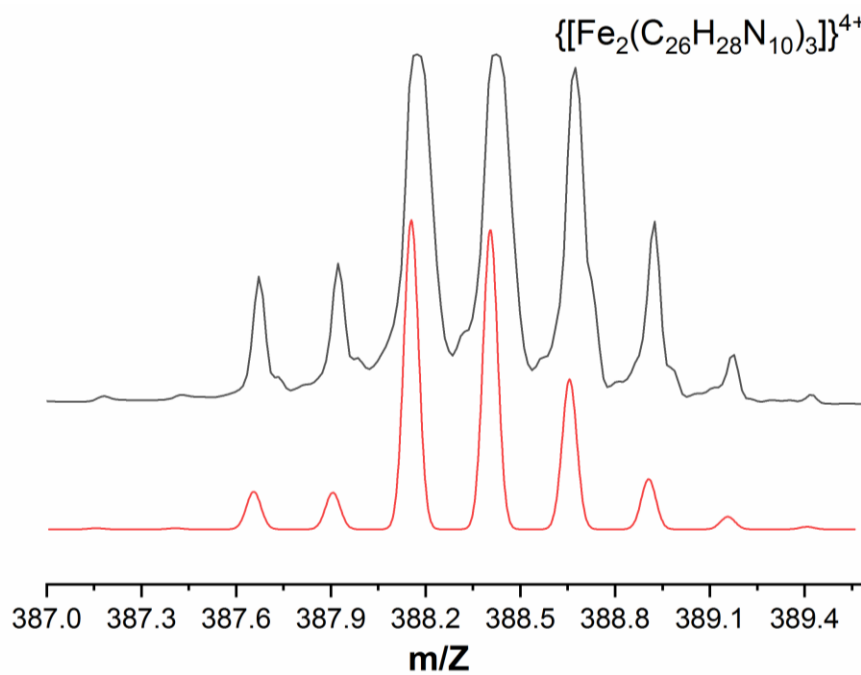


Figure S11. Fit of a peak in the mass spectrum of $[\text{Fe}_2(\text{L}^4\text{pym-meta})_3](\text{BF}_4)_4$ (**2**) (Figure S10): $[\text{Fe}_2(\text{L}^4\text{pym-meta})_3]^{4+}$ experimental (black) and simulated pattern (red).

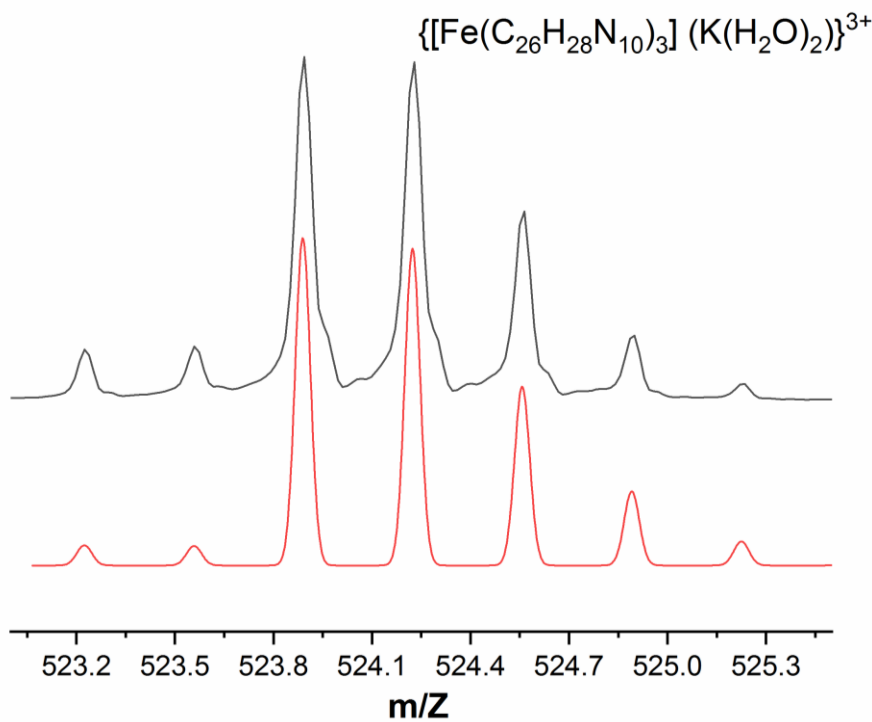


Figure S12. Fit of a peak in the mass spectrum of $[\text{Fe}_2(\text{L}^4\text{pym-meta})_3](\text{BF}_4)_4$ (**2**) (Figure S10): $\{[\text{FeL}^4\text{pym-meta}]_3\}(\text{K}(\text{H}_2\text{O})_2)^{3+}$ experimental (black) and simulated pattern (red).

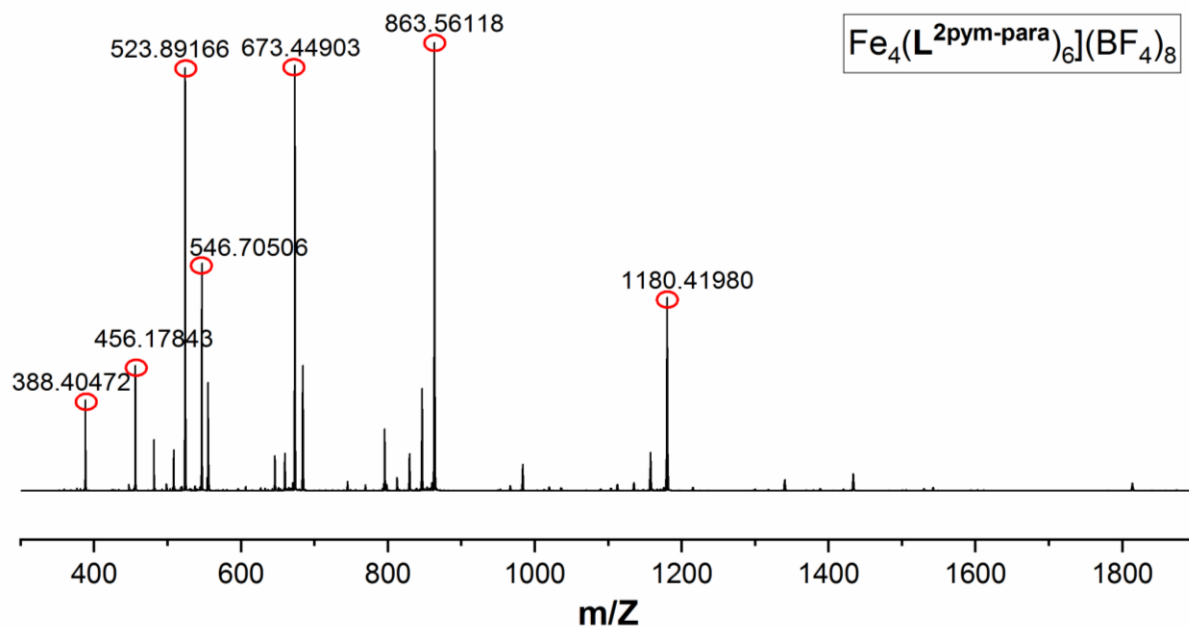


Figure S13. Mass spectrum of $[\text{Fe}_4(\text{L}^{2\text{pym-para}})_6](\text{BF}_4)_8$ (**3**). Fits of the circled peaks are provided in the following figures.

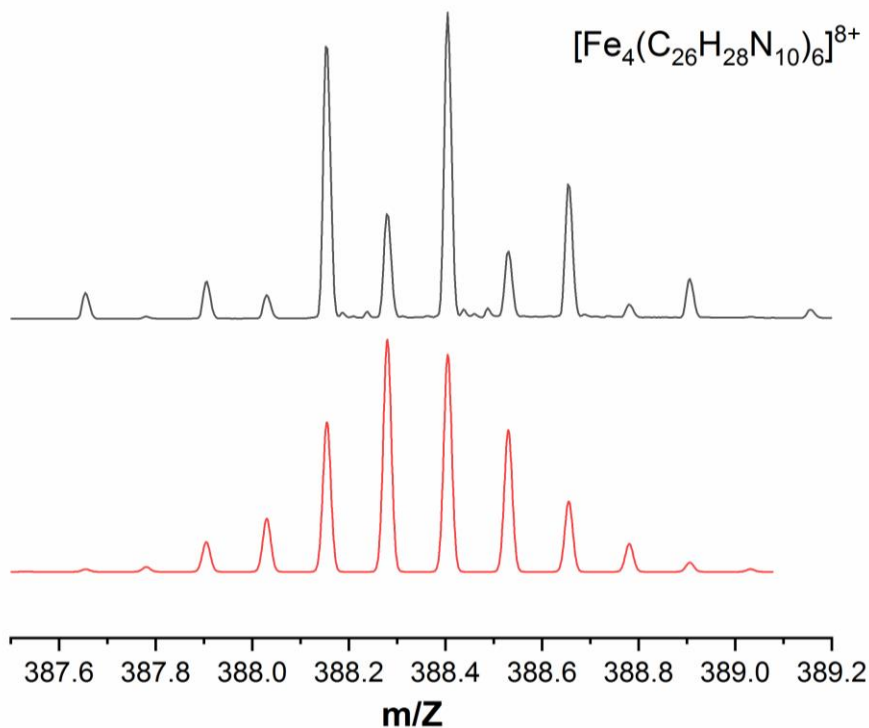


Figure S14. Fit of a peak in the mass spectrum of $[\text{Fe}_4(\text{L}^{2\text{pym-para}})_6](\text{BF}_4)_8$ (**3**) (Figure S13): $[\text{Fe}_4(\text{L}^{2\text{pym-para}})_6]^{8+}$ experimental (black) and simulated pattern (red).

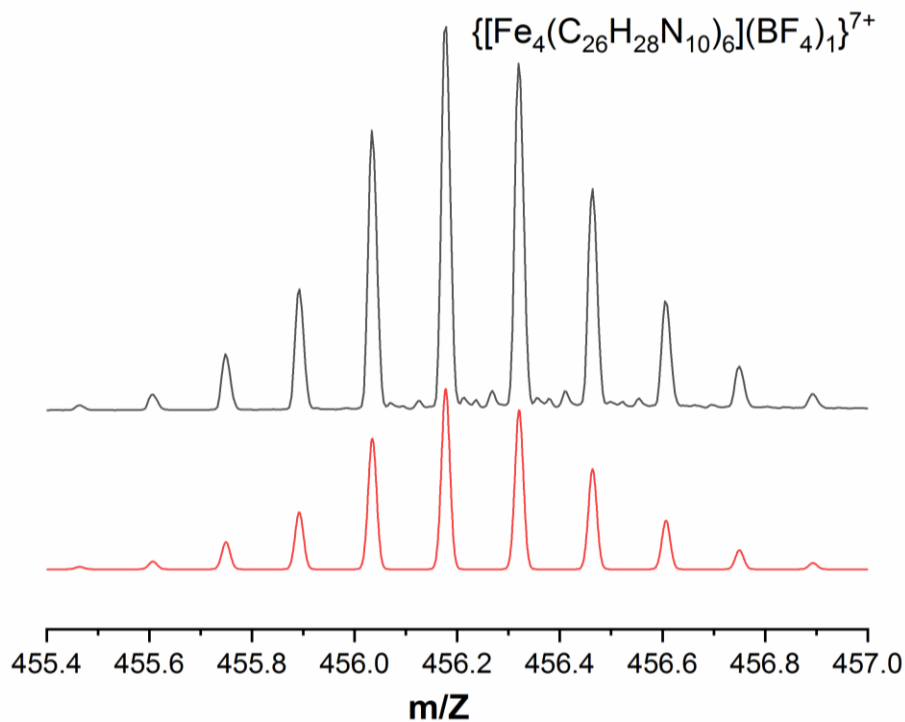


Figure S15. Fit of a peak in the mass spectrum of $[\text{Fe}_4(\text{L}^{2\text{pym-para}})_6](\text{BF}_4)_8$ (**3**) (Figure S13): $[\text{Fe}_4(\text{L}^{2\text{pym-para}})_6](\text{BF}_4)_1\}^{7+}$ experimental (black) and simulated pattern (red).

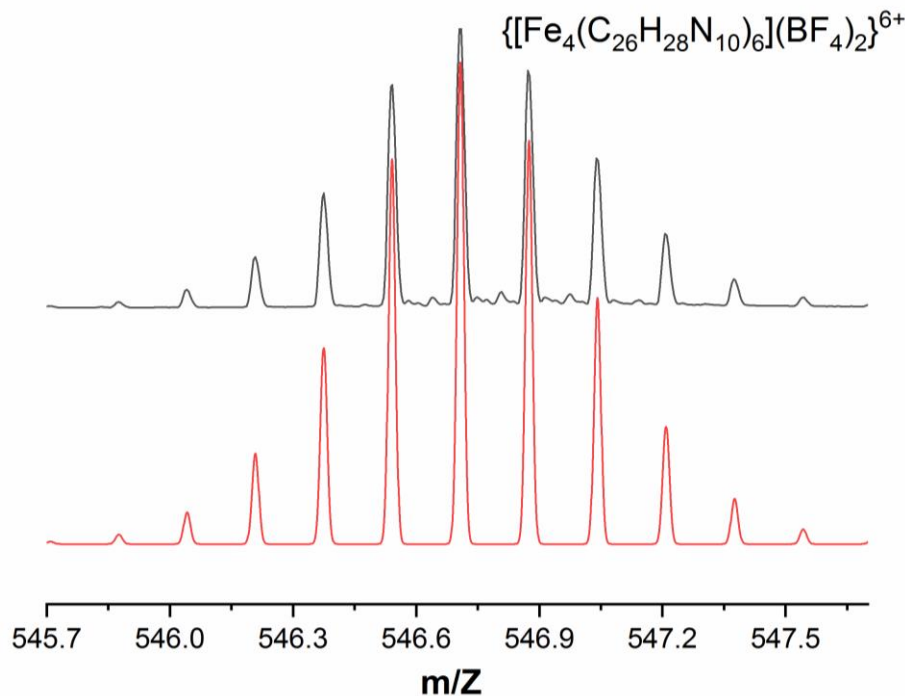


Figure S16. Fit of a peak in the mass spectrum of $[\text{Fe}_4(\text{L}^{2\text{pym-para}})_6](\text{BF}_4)_8$ (**3**) (Figure S13): $[\text{Fe}_4(\text{L}^{2\text{pym-para}})_6](\text{BF}_4)_2\}^{6+}$ experimental (black) and simulated pattern (red).

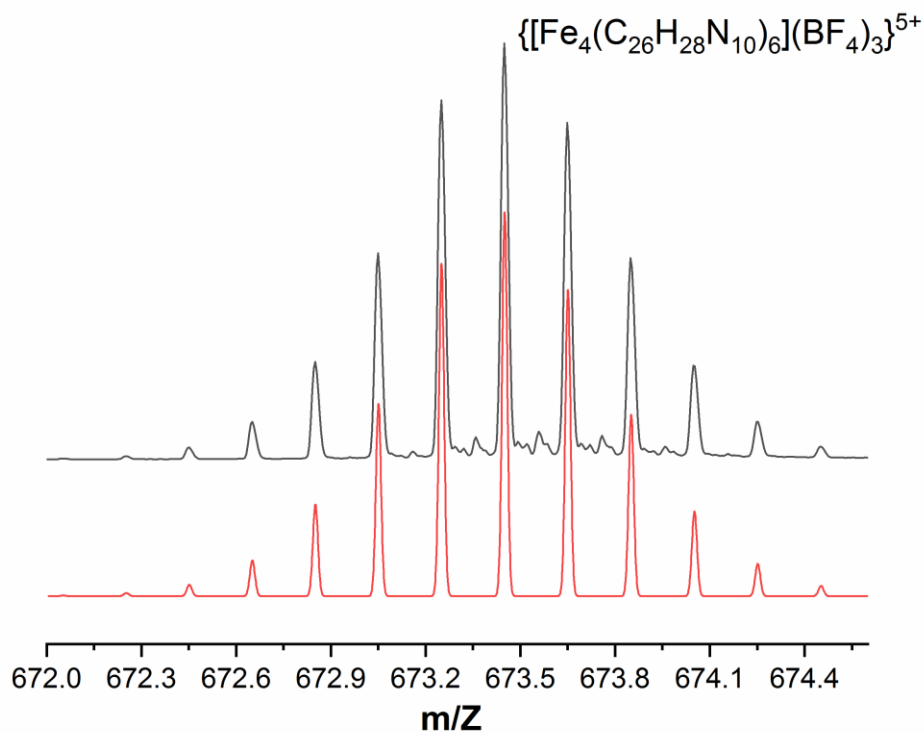


Figure S17. Fit of a peak in the mass spectrum of $[\text{Fe}_4(\text{L}^{2\text{pym-para}})_6](\text{BF}_4)_8$ (**3**) (Figure S13): $[\text{Fe}_4(\text{L}^{2\text{pym-para}})_6](\text{BF}_4)_3\}^{5+}$ experimental (black) and simulated pattern (red).

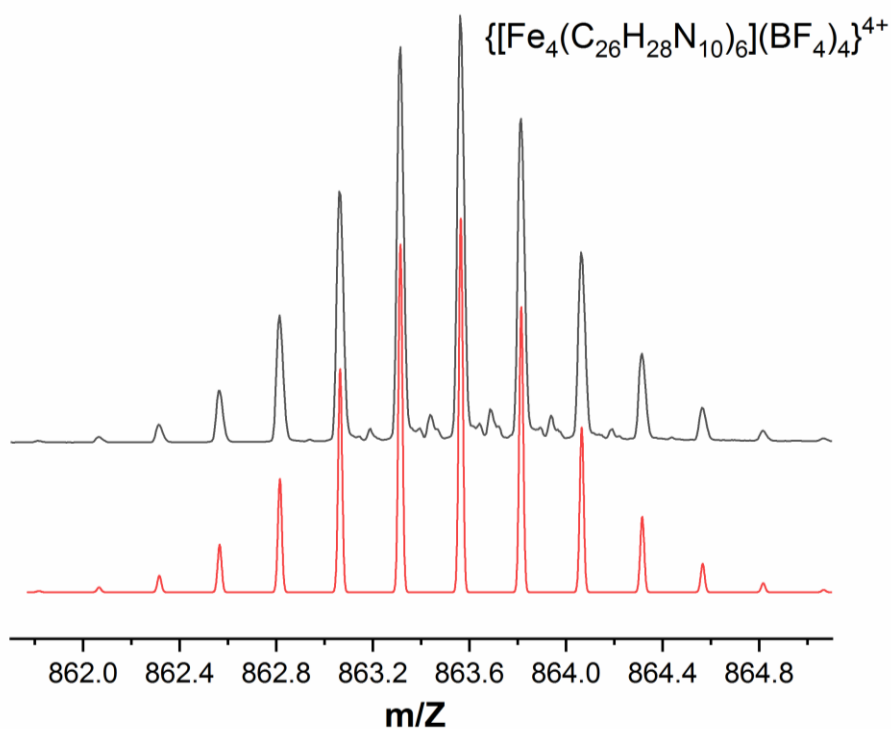


Figure S18. Fit of a peak in the mass spectrum of $[\text{Fe}_4(\text{L}^{2\text{pym-para}})_6](\text{BF}_4)_8$ (**3**) (Figure S13): $[\text{Fe}_4(\text{L}^{2\text{pym-para}})_6](\text{BF}_4)_4\}^{4+}$ experimental (black) and simulated pattern (red).

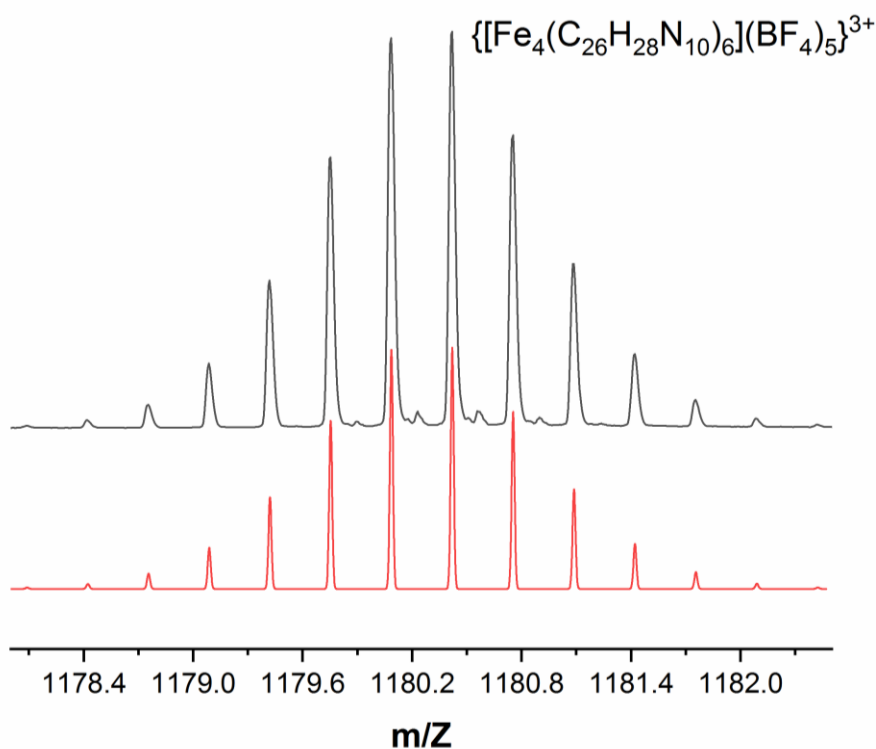


Figure S19. Fit of a peak in the mass spectrum of $[\text{Fe}_4(\text{L}^{2\text{pym-para}})_6](\text{BF}_4)_8$ (**3**) (Figure S13): $[\text{Fe}_4(\text{L}^{2\text{pym-para}})_6](\text{BF}_4)_5\}^{3+}$ experimental (black) and simulated pattern (red).

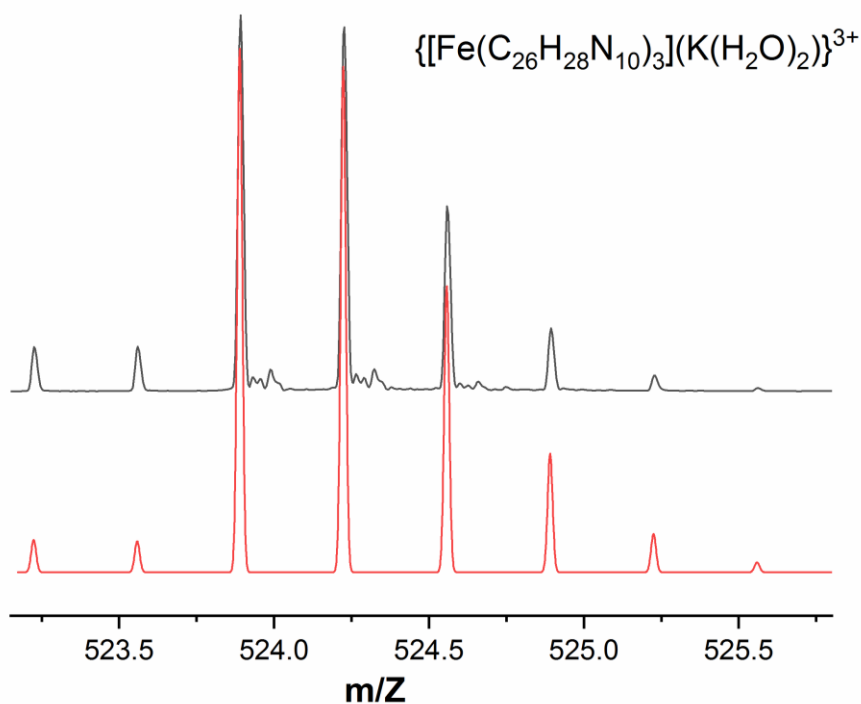


Figure S20. Fit of a peak in the mass spectrum of $[\text{Fe}_4(\text{L}^{2\text{pym-para}})_6](\text{BF}_4)_8$ (**3**) (Figure S13): $[\text{Fe}(\text{L}^{2\text{pym-para}})_3](\text{K}(\text{H}_2\text{O})_2)\}^{3+}$ experimental (black) and simulated pattern (red).

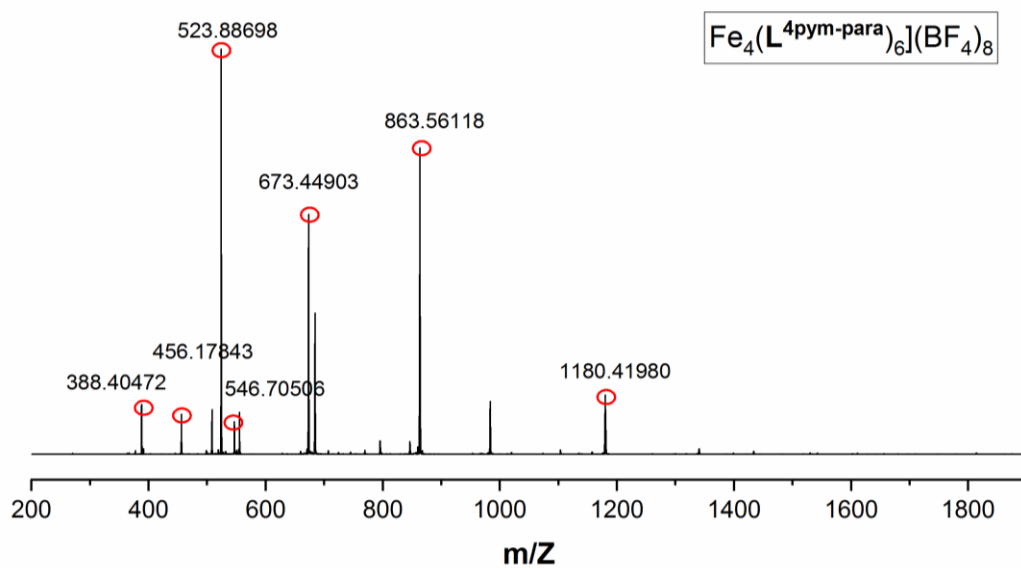


Figure S21. Mass spectrum of $[\text{Fe}_4(\text{L}^4\text{pym-para})_6](\text{BF}_4)_8$. Fits of the circled peaks are provided in the following figures.

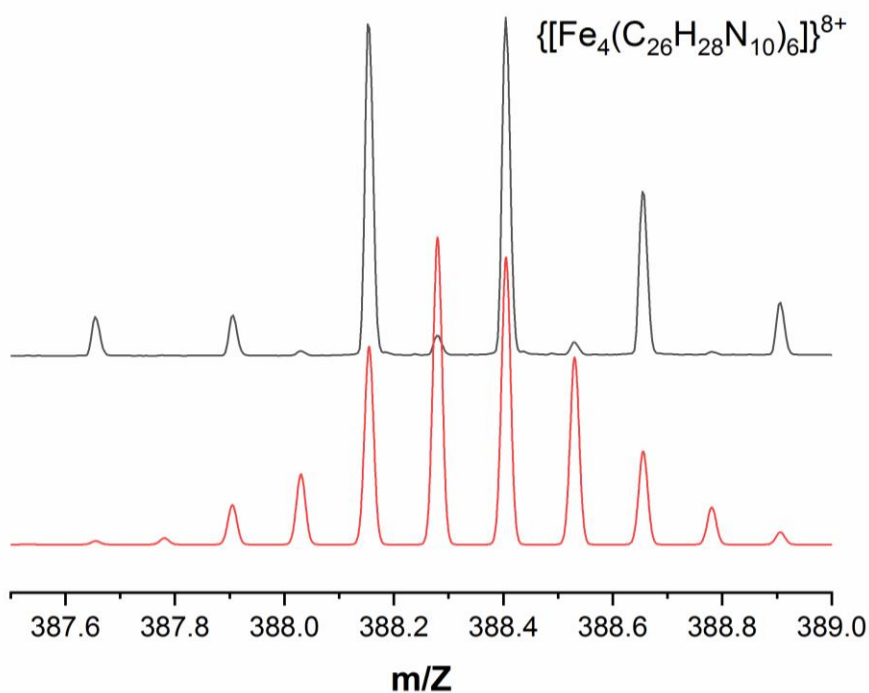


Figure S22. Fit of a peak in the mass spectrum of $[\text{Fe}_4(\text{L}^4\text{pym-para})_6](\text{BF}_4)_8$ (**4**) (Figure S21): $[\text{Fe}_4(\text{L}^4\text{pym-para})_6]^{8+}$ experimental (black) and simulated pattern (red).

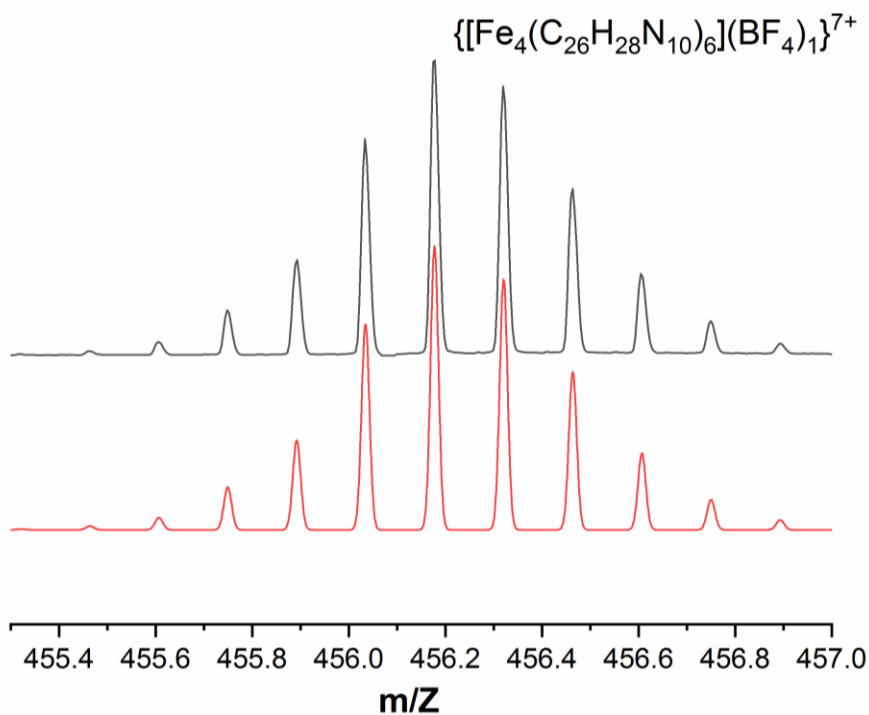


Figure S23. Fit of a peak in the mass spectrum of $[\text{Fe}_4(\text{L}^{4\text{pym-para}})_6](\text{BF}_4)_8$ (**4**) (Figure S21): $[\text{Fe}_4(\text{L}^{4\text{pym-para}})_6](\text{BF}_4)_1\}^{7+}$ experimental (black) and simulated pattern (red).

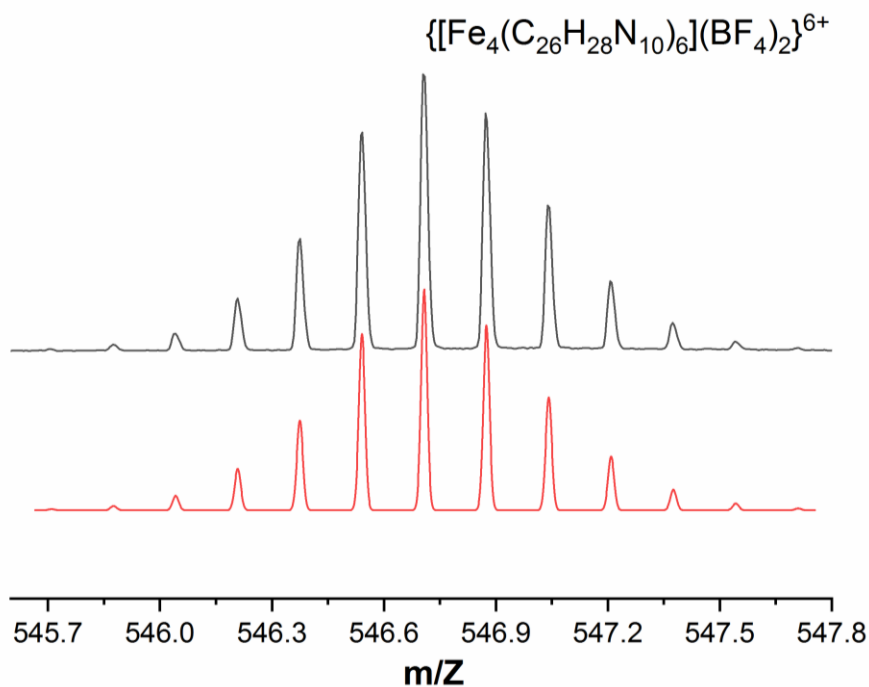


Figure S24. Fit of a peak in the mass spectrum of $[\text{Fe}_4(\text{L}^{4\text{pym-para}})_6](\text{BF}_4)_8$ (**4**) (Figure S21): $[\text{Fe}_4(\text{L}^{4\text{pym-para}})_6](\text{BF}_4)_2\}^{6+}$ experimental (black) and simulated pattern (red).

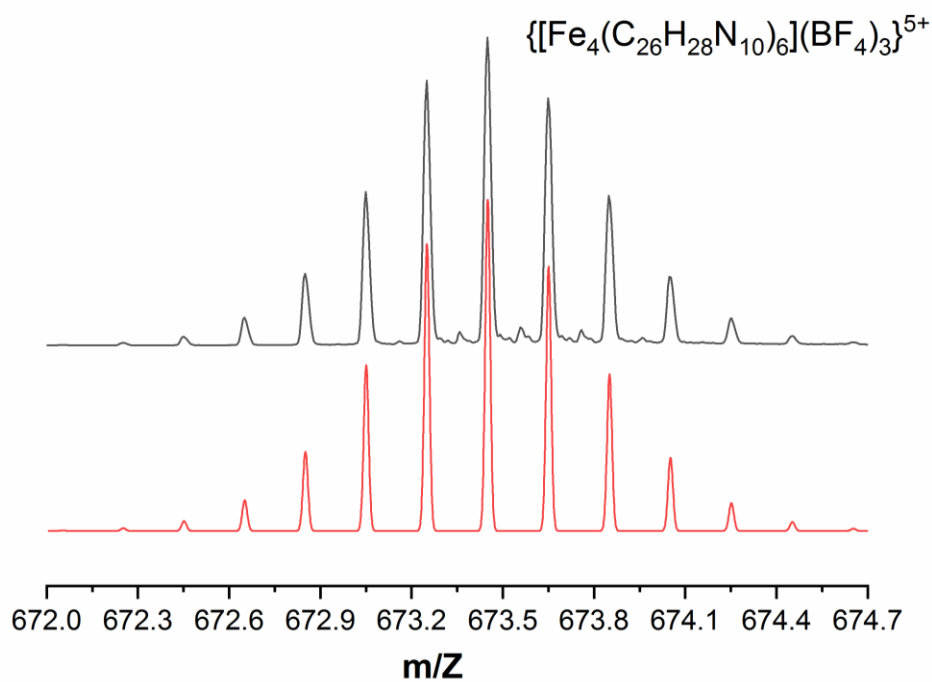


Figure S25. Fit of a peak in the mass spectrum of $[\text{Fe}_4(\text{L}^{\text{4pym-para}})_6](\text{BF}_4)_8$ (**4**) (Figure S21): $[\text{Fe}_4(\text{L}^{\text{4pym-para}})_6](\text{BF}_4)_3^{5+}$ experimental (black) and simulated pattern (red).

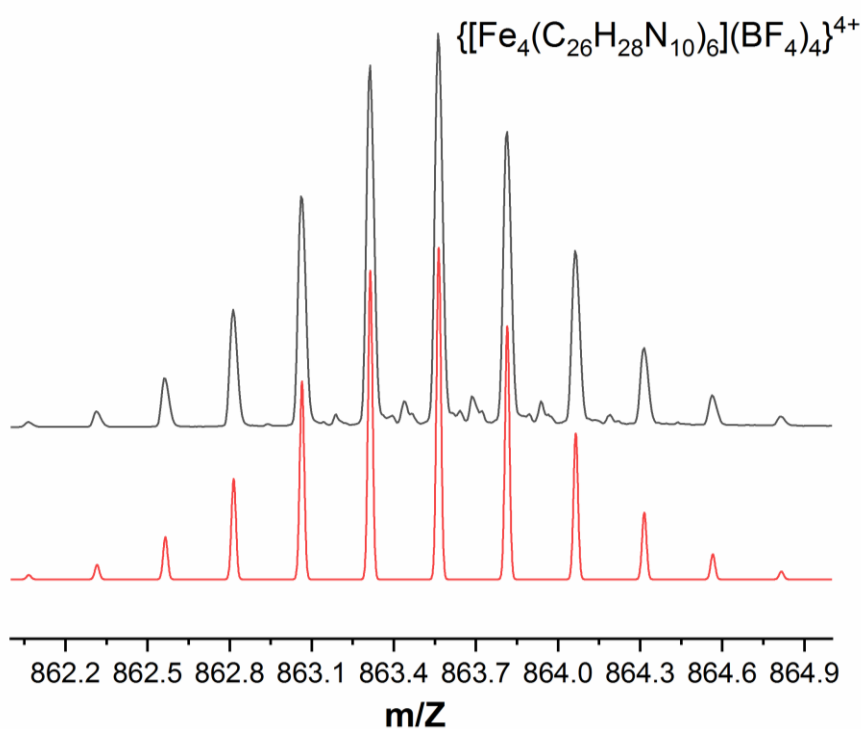


Figure S26. Fit of a peak in the mass spectrum of $[\text{Fe}_4(\text{L}^{\text{4pym-para}})_6](\text{BF}_4)_8$ (**4**) (Figure S21): $[\text{Fe}_4(\text{L}^{\text{4pym-para}})_6](\text{BF}_4)_4^{4+}$ experimental (black) and simulated pattern (red).

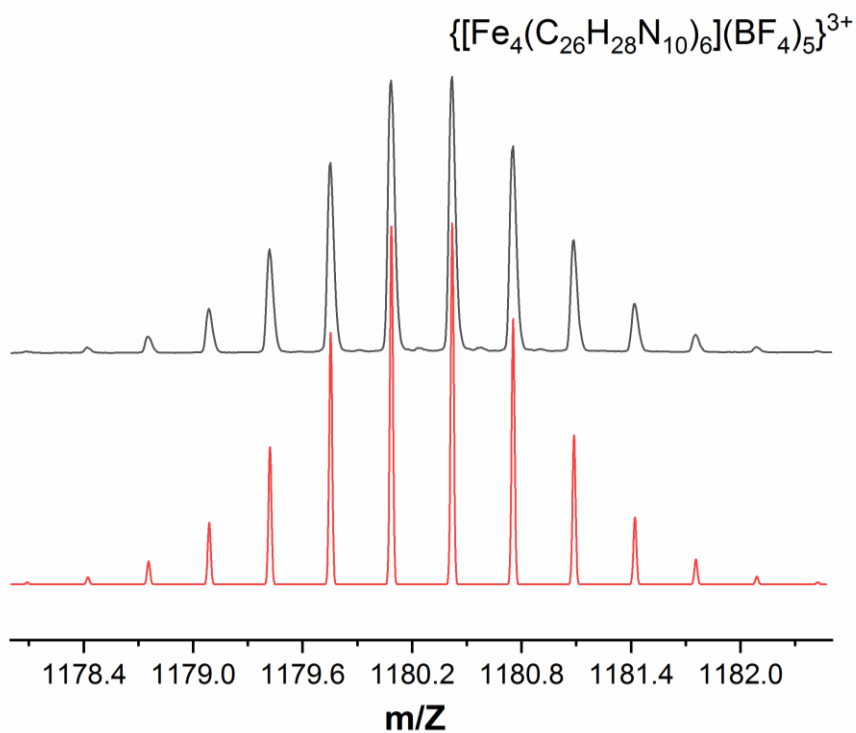


Figure S27. Fit of a peak in the mass spectrum of $[\text{Fe}_4(\text{L}^{\text{4pym-para}})_6](\text{BF}_4)_8$ (**4**) (Figure S21): $[\text{Fe}_4(\text{L}^{\text{4pym-para}})_6](\text{BF}_4)_5\}^{3+}$ experimental (black) and simulated pattern (red).

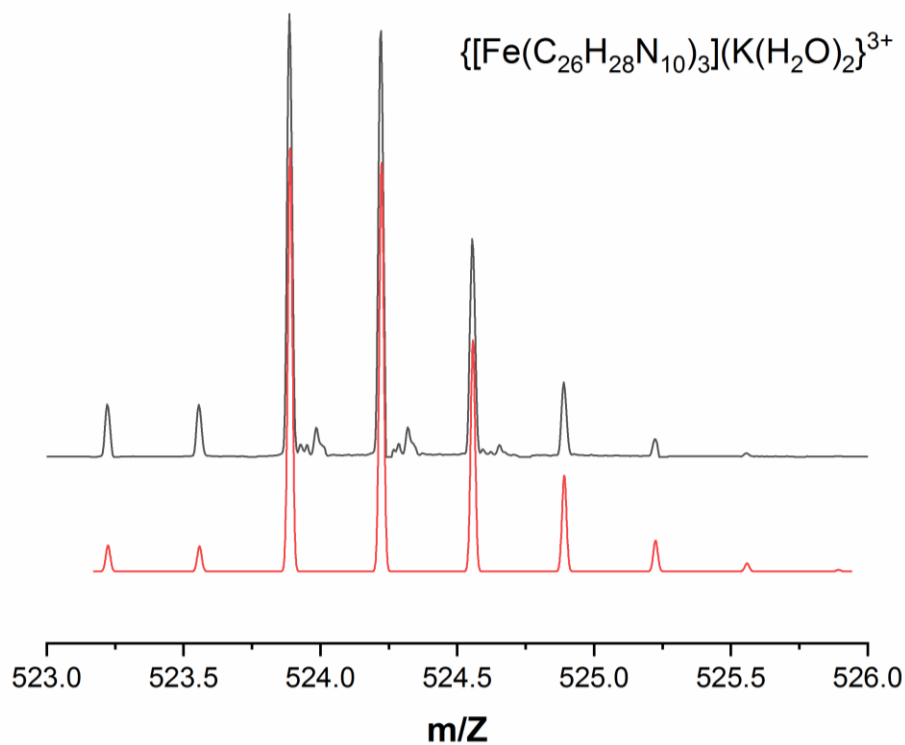


Figure S28. Fit of a peak in the mass spectrum of $[\text{Fe}_4(\text{L}^{\text{4pym-para}})_6](\text{BF}_4)_8$ (**4**) (Figure S21): $[\text{Fe}(\text{L}^{\text{4pym-para}})_3](\text{K}(\text{H}_2\text{O})_2)\}^{3+}$ experimental (black) and simulated pattern (red).

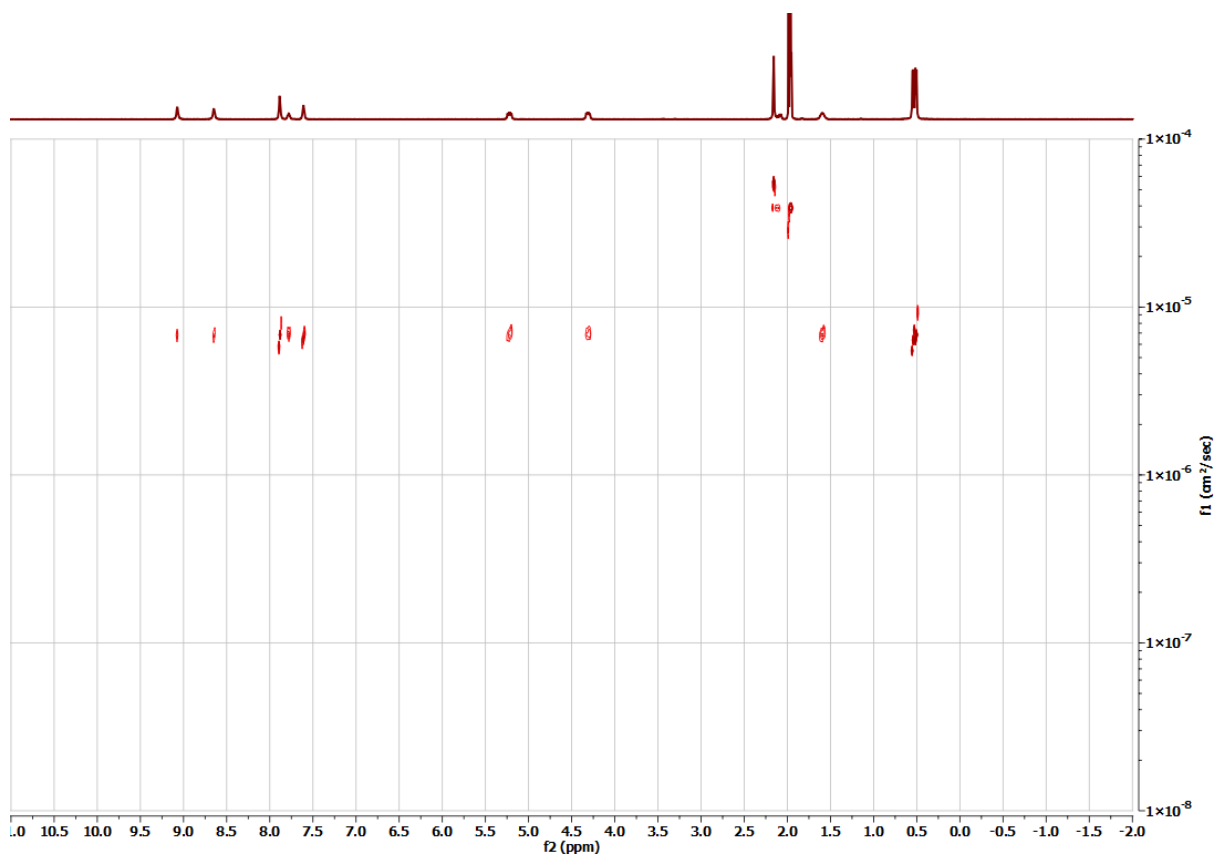


Figure S29. ¹H DOSY-NMR spectrum (500 MHz) of Fe₂(L²pym-meta)₃(BF₄)₄ (**1**) in CD₃CN at 25 °C.

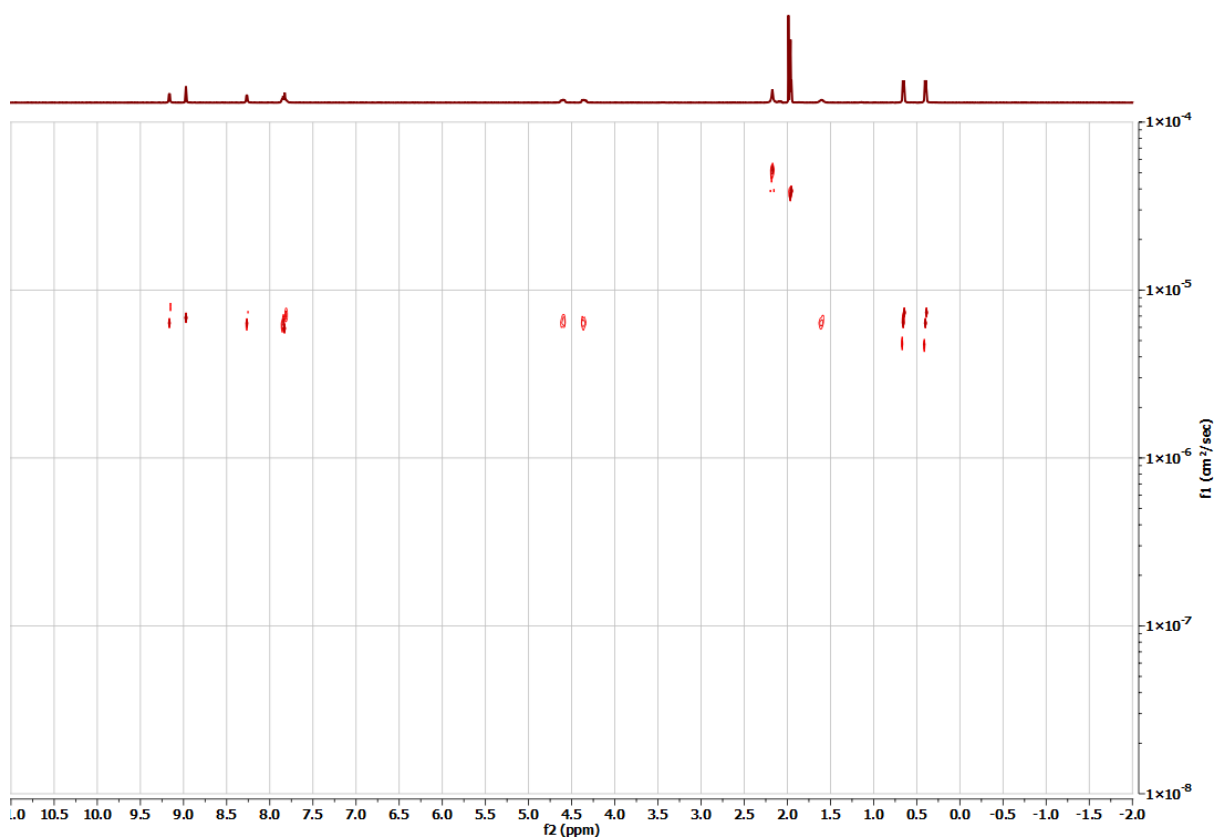


Figure S30. ¹H DOSY-NMR spectrum (500 MHz) of Fe₂(L⁴pym-meta)₃(BF₄)₄ (**2**) in CD₃CN at 25 °C.

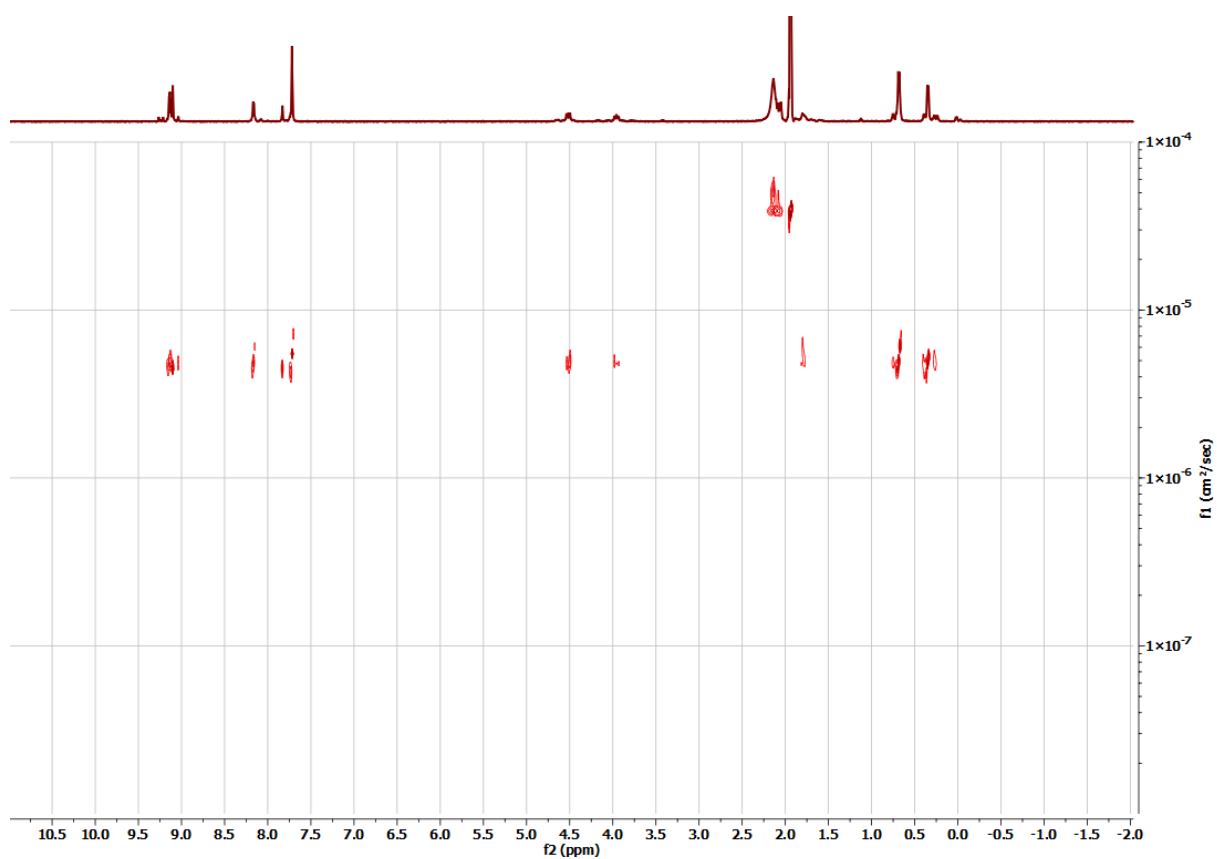


Figure S31. ^1H DOSY-NMR spectrum (500 MHz) of $\text{Fe}_4(\text{L}^2\text{pym-para})_6(\text{BF}_4)_8$ (**3**) in CD_3CN at 25 °C.

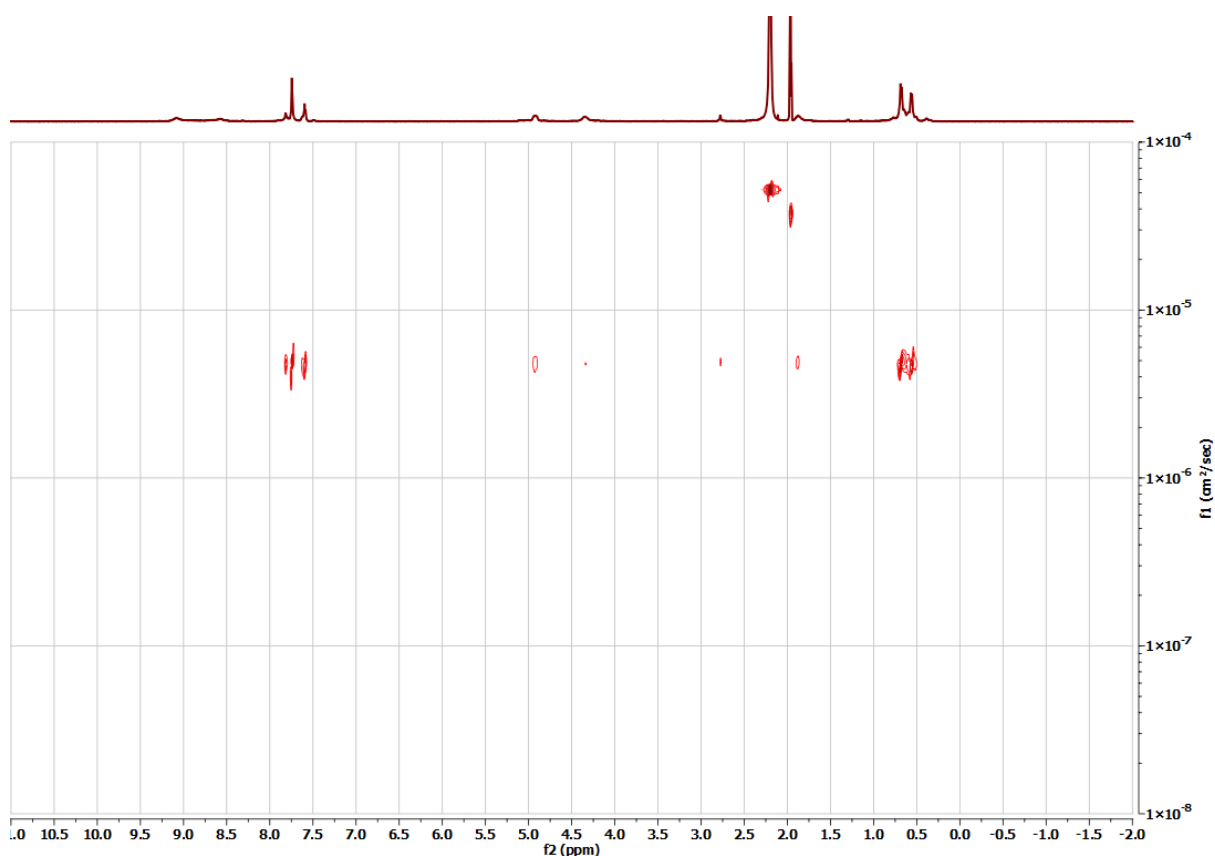


Figure S32. ^1H DOSY-NMR spectrum (500 MHz) of $\text{Fe}_4(\text{L}^4\text{pym-para})_6(\text{BF}_4)_8$ (**4**) in CD_3CN at 25 °C.

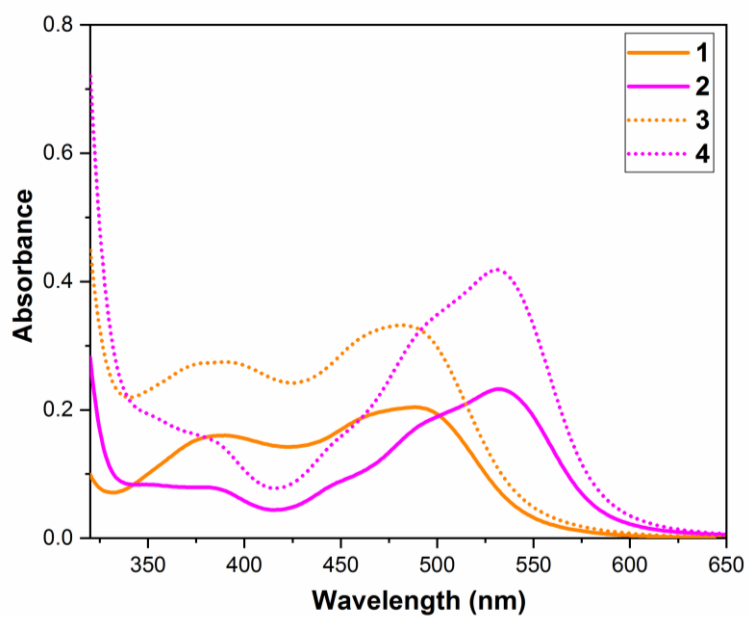


Figure S33a. UV-vis studies of 0.01mM acetonitrile solutions of complexes **1-4** at room temperature, absorbance vs wavelength (extinction coefficient plot in main paper).

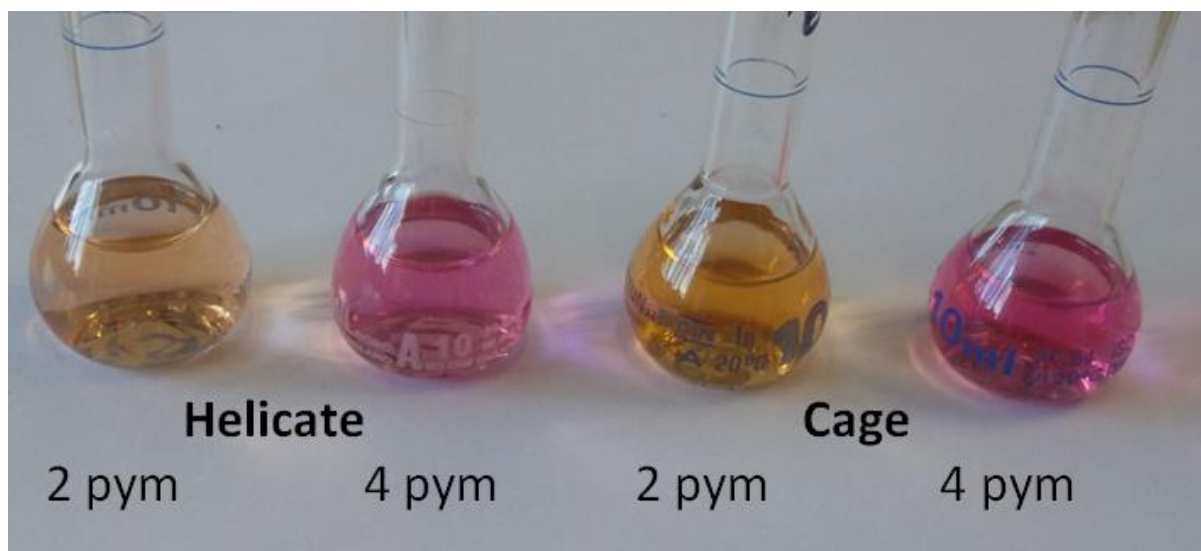


Figure S33b. 0.01mM solutions of **1-4** in acetonitrile at room temperature for UV-vis studies.

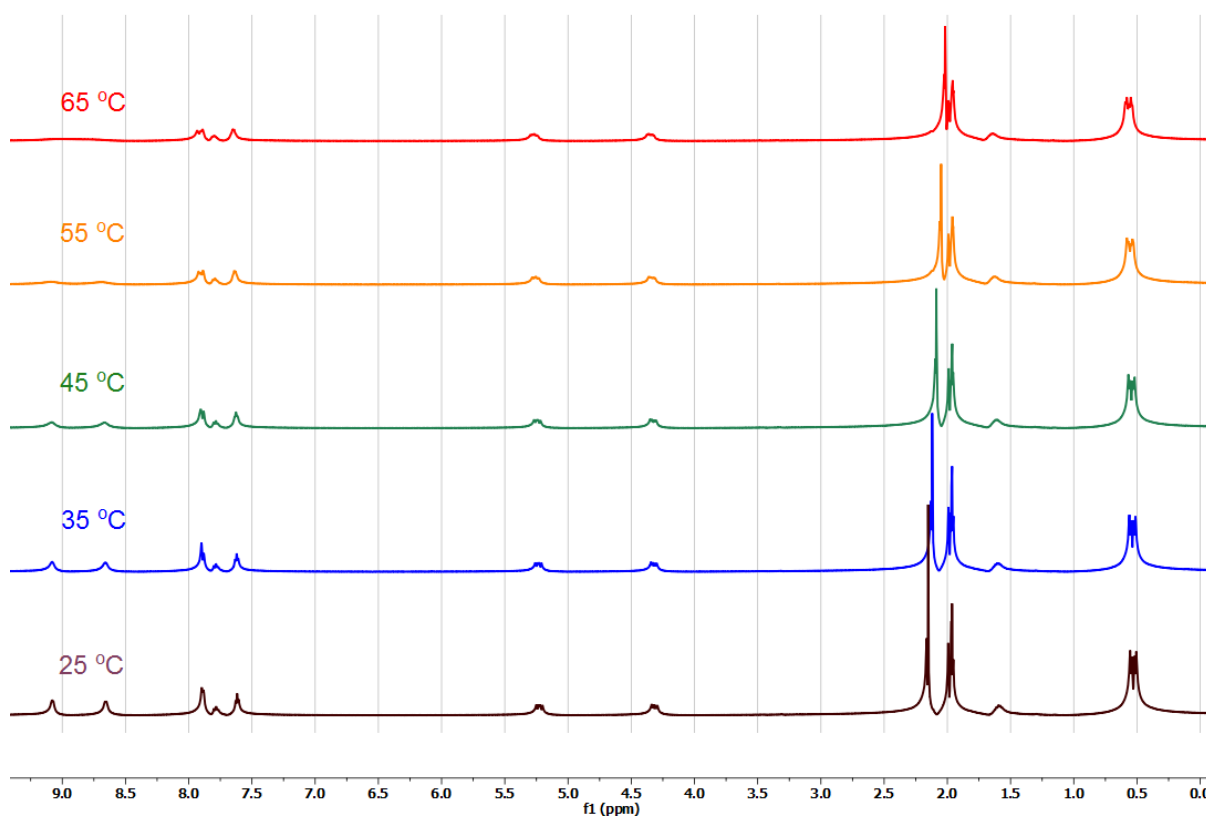


Figure S34. Evans method ^1H NMR spectra (500 MHz) of $\text{Fe}_2(\text{L}^{2\text{pym-meta}})_3(\text{BF}_4)_4$ (**1**) in CD_3CN in 10° steps from 25-65 $^\circ\text{C}$. The solvent signals from the inner capillary (pure solvent) and outer solution (includes complex in the same solvent) overlaid one another, consistent with the complex being diamagnetic in this solvent in this temperature range.

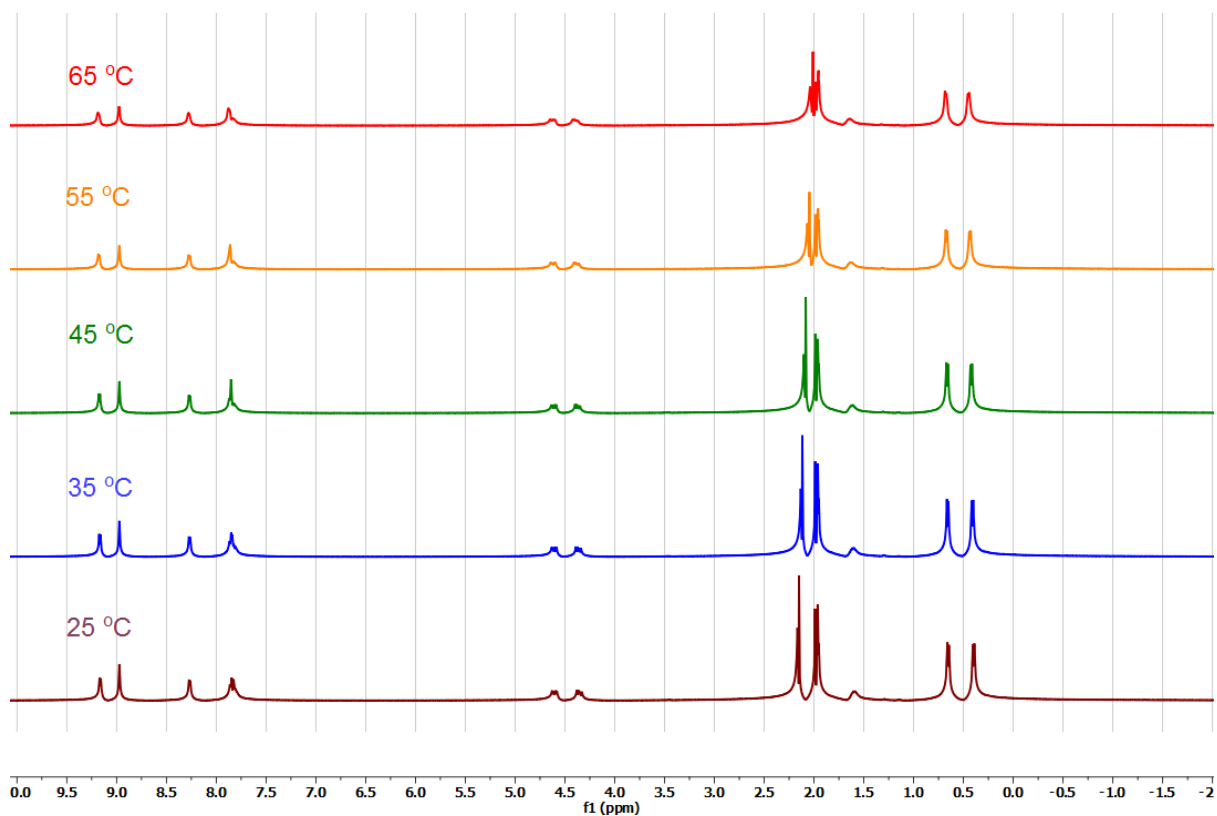


Figure S35. Evans method ^1H NMR spectra (500 MHz) of $\text{Fe}_2(\text{L}^{4\text{pym-meta}})_3(\text{BF}_4)_4$ (**2**) in CD_3CN in 10° steps from 25-65°C. The solvent signals from the inner capillary (pure solvent) and outer solution (includes complex in the same solvent) overlaid one another, consistent with the complex being diamagnetic in this solvent in this temperature range.

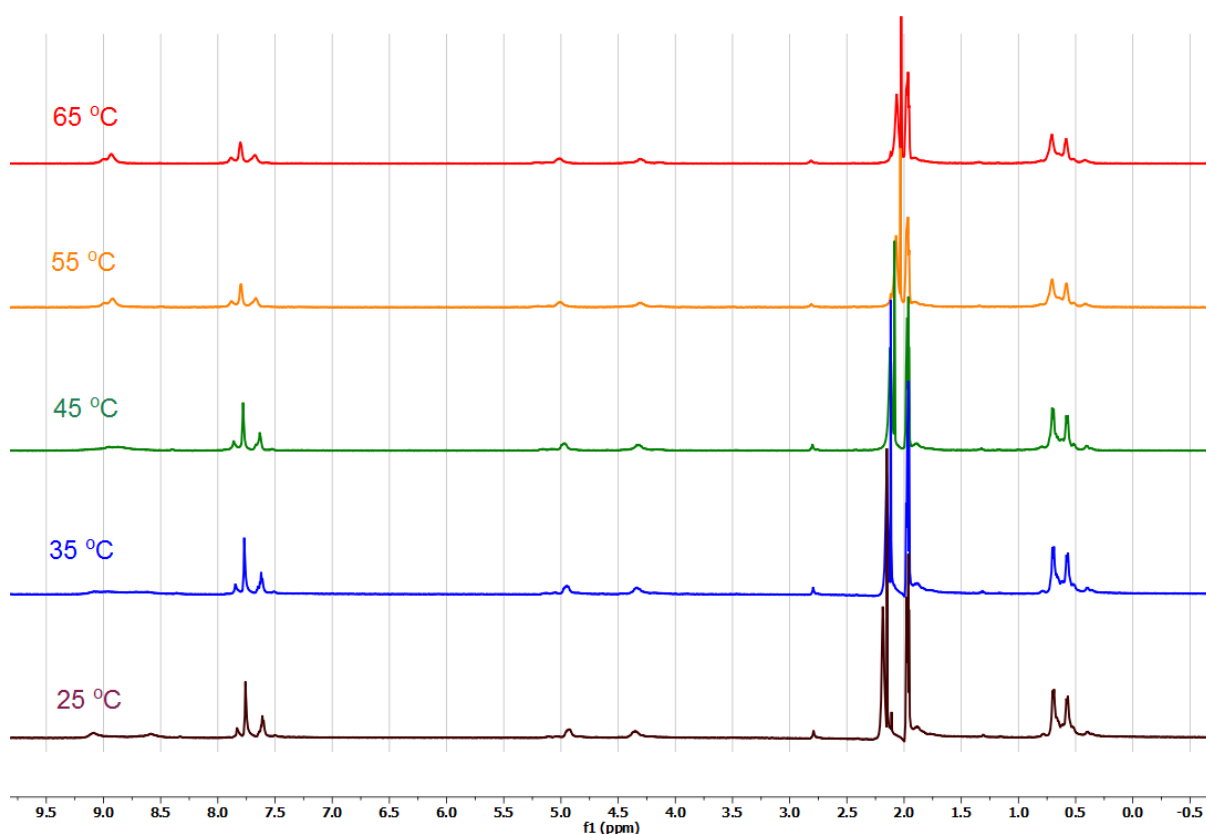


Figure S36. Evans method ¹H NMR spectra (500 MHz) of Fe₄(L^{2pym-para})₆(BF₄)₈ (**3**) in CD₃CN in 10° steps from 25-65°C. The solvent signals from the inner capillary (pure solvent) and outer solution (includes complex in the same solvent) overlaid one another, consistent with the complex being diamagnetic in this solvent in this temperature range.

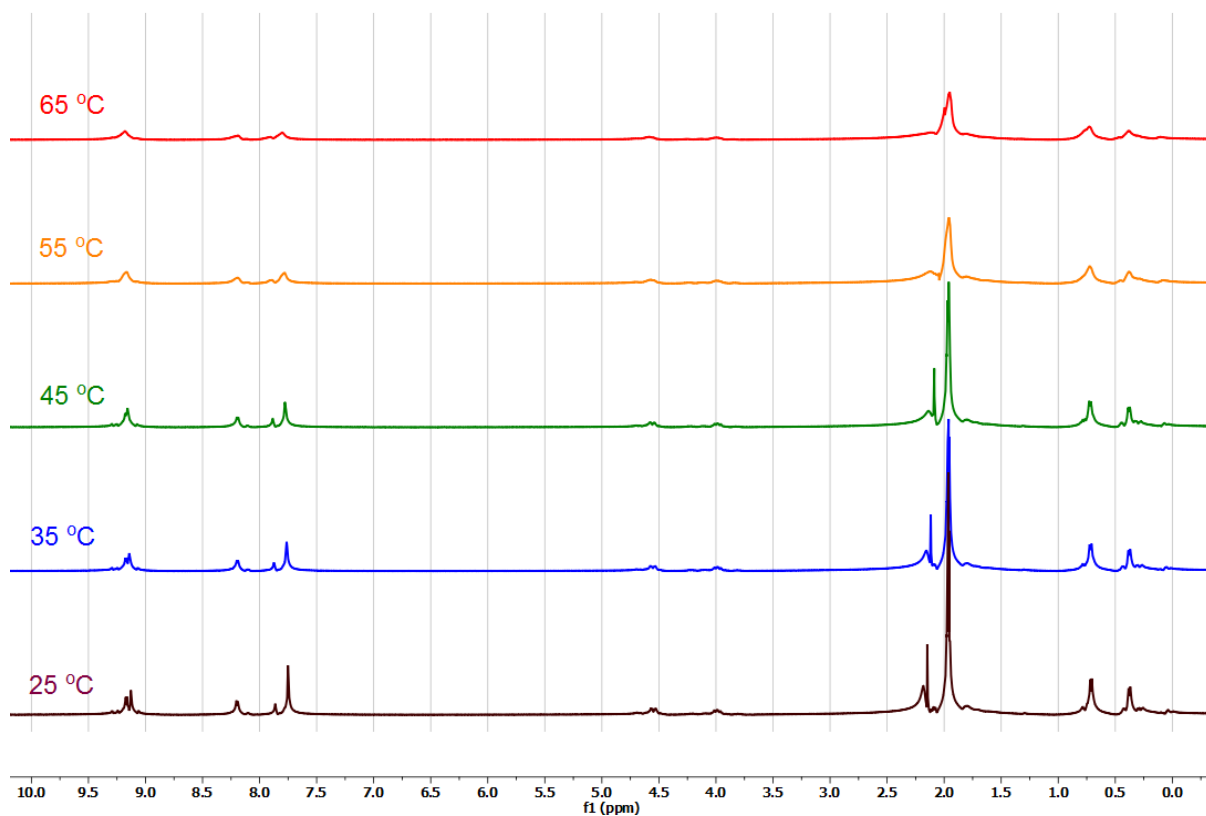


Figure S37. Evans method ^1H NMR spectra (500 MHz) of $\text{Fe}_4(\text{L}^{4\text{pym-para}})_6(\text{BF}_4)_4$ (**4**) in CD_3CN in 10° steps from 25-65°C. The solvent signals from the inner capillary (pure solvent) and outer solution (includes complex in the same solvent) overlaid one another, consistent with the complex being diamagnetic in this solvent in this temperature range.

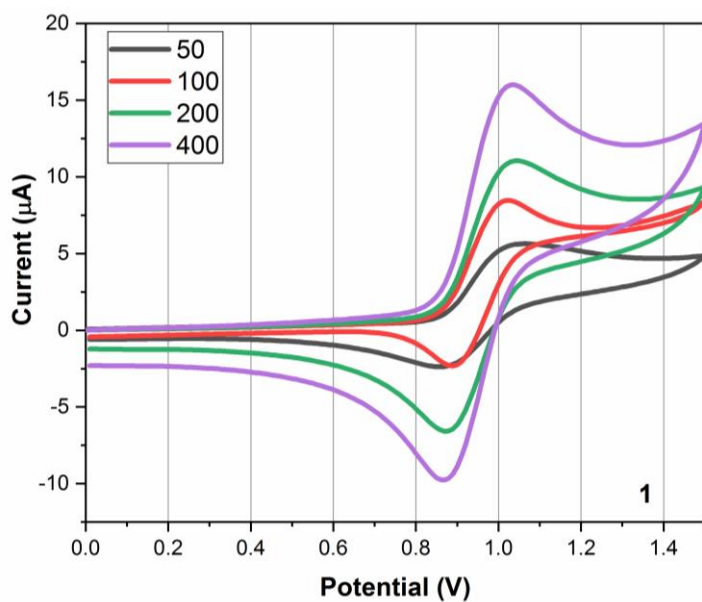


Figure S38. CVs of 1 mM of $[\text{Fe}_2(\text{L}^{2\text{pym-meta}})_3](\text{BF}_4)_4$ (**1**) in MeCN, from 0 → +1.5 → 0 V vs 0.01 M Ag/AgNO₃ at scan rates 50, 100, 200 and 400 mV s⁻¹.

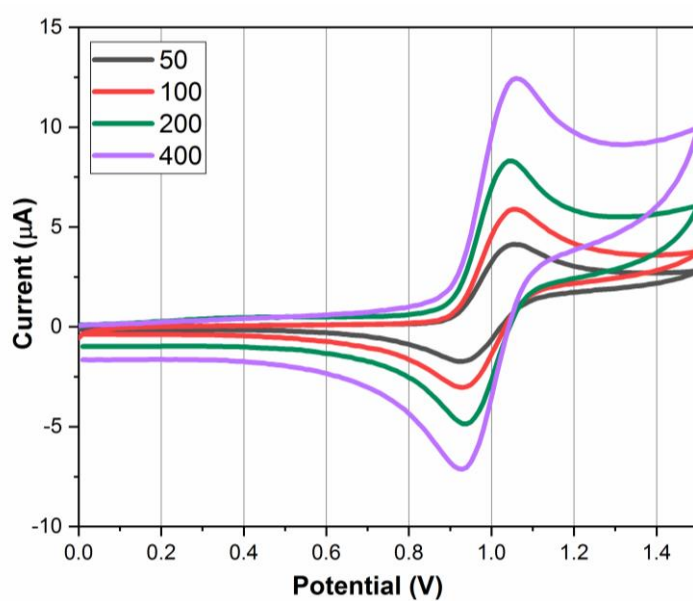


Figure S39. CVs of 1 mM of $[\text{Fe}_2(\text{L}^{4\text{pym-meta}})_3](\text{BF}_4)_4$ (**2**) in MeCN, from 0 → +1.5 → 0 V vs 0.01 M Ag/AgNO₃ at scan rates 50, 100, 200 and 400 mV s⁻¹.

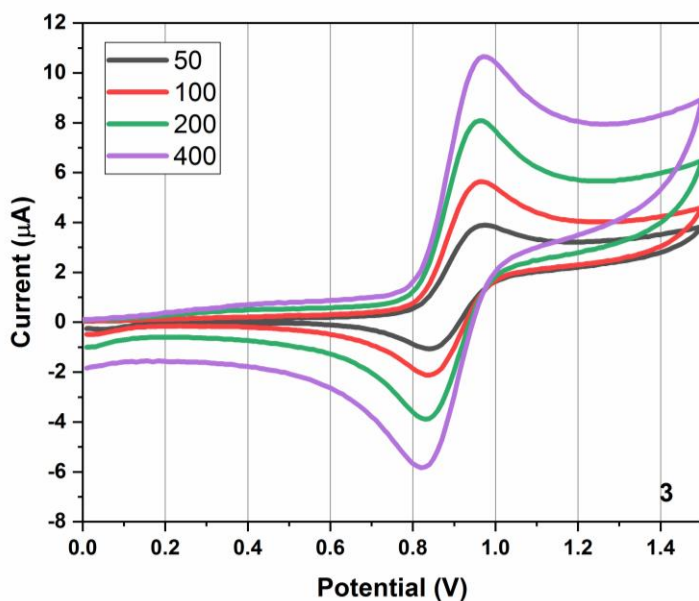


Figure S40. CVs of 0.05 mM of $[\text{Fe}_4(\text{L}^{2\text{pym-meta}})_6](\text{BF}_4)_8$ (**3**) in MeCN, from 0 \rightarrow +1.5 \rightarrow 0 V vs 0.01M Ag/AgNO₃ at scan rates 50, 100, 200 and 400 mV s⁻¹.

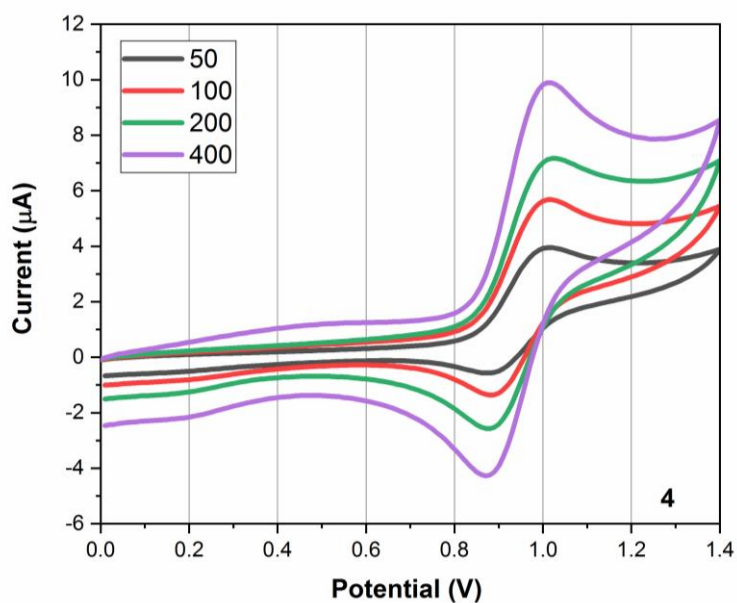


Figure S41. CVs of 0.05 mM of $[\text{Fe}_4(\text{L}^{4\text{pym-para}})_6](\text{BF}_4)_8$ (**4**) in MeCN, from 0 \rightarrow +1.4 \rightarrow 0 V vs 0.01M Ag/AgNO₃ at scan rates 50, 100, 200 and 400 mV s⁻¹.

Table S6. Summary of reversible/quasi-reversible single electron oxidation-reduction process of **1-4** complexes at 200 mVs⁻¹ scan rate.

Complex	$i_{pa}(\mu A)$	$i_{pc}(\mu A)$	i_{pa}/i_{pc}
1	10.657	10.263	1.03
2	7.850	7.815	1.00
3	6.760	7.564	0.894
4	5.284	6.085	0.868

Table S7. Microanalysis and TGA of all complexes.

	C ($\Delta\%$)	H ($\Delta\%$)	N ($\Delta\%$)	TGA ($\Delta\%$)
1 ·5H ₂ O·4CH ₃ CN (cal.)	47.72 (0.21)	4.73 (0.23)	22.22 (-0.12)	11.3 (0.5)
	47.93	4.96	22.10	11.8
2 ·3H ₂ O·2CH ₃ CN (cal.)	48.63 (-0.27)	4.85 (-0.10)	21.78 (0.23)	7 (0.3)
	48.36	4.75	22.01	6.7
3 ·7H ₂ O·5CH ₃ NO ₂ (cal.)	45.43 (0.31)	4.76 (-0.18)	21.17 (0.37)	9.6 (0.5)
	45.74	4.58	21.54	10.1
4 ·9H ₂ O (cal.)	47.34 (-0.06)	4.95 (-0.22)	21.05 (0.15)	4.7 (0.6)
	47.28	4.73	21.20	4.1

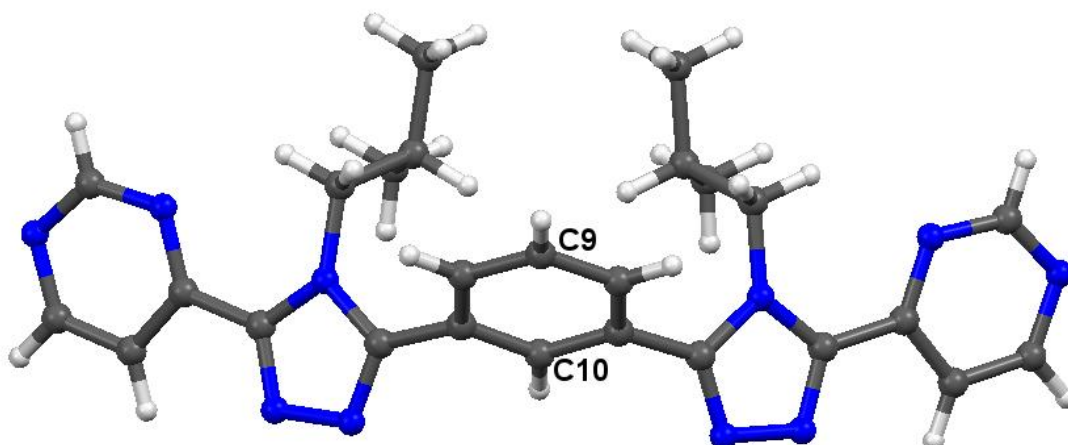


Figure S42. Crystal structure of $L^{4pym-meta}$. A mirror plane passes through C9 and C10, so only half of the molecule is present in the asymmetric unit.

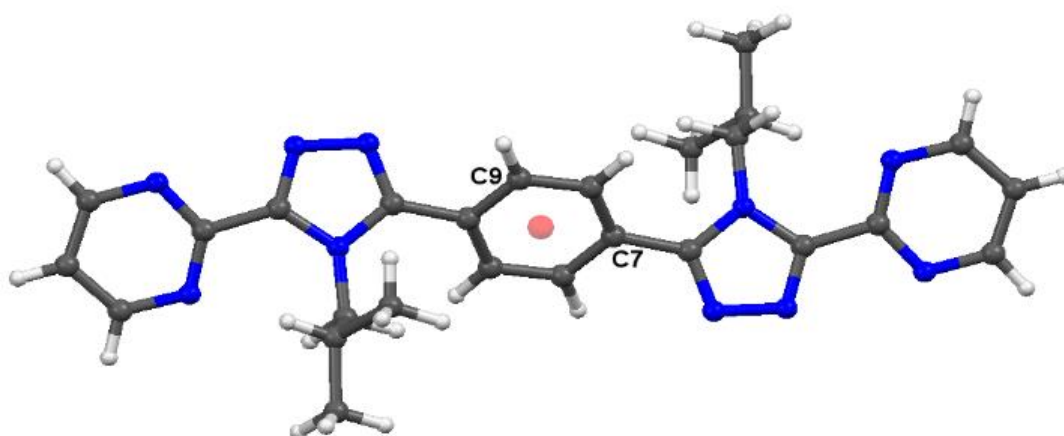


Figure S43. Crystal structure of $L^{2pym-para}$. A centre of inversion present (location shown by a pink dot), so only half of the molecule is present in the asymmetric unit.

Table S8. Crystal Data and Structure Refinement Details for the Ligands.

	L⁴pym-meta	L²pym-para
Empirical formula	C ₂₆ H ₂₈ N ₁₀	C ₂₆ H ₂₈ N ₁₀
M _r	480.58	480.58
Crystal system	monoclinic	monoclinic
Space group	P 2 ₁ /m	C 2/m
a [Å]	6.3326(2)	25.6375(7)
b [Å]	25.1899(7)	6.4752(2)
c [Å]	8.0053(3)	15.2392(4)
α [°]	90	90
β [°]	111.628(5)	104.216(3)
γ [°]	90	90
V [Å ³]	1187.08(8)	2452.36(12)
Z	2	4
T [K]	100	100
ρ _{calcd.} [g/cm ³]	1.345	1.302
μ [mm ⁻¹]	0.688	0.666
F(000)	508.0	1016.0
Crystal Size (mm)	0.4 × 0.2 × 0.2	0.4 × 0.2 × 0.2
2θ range for data collection (Cu radiation)	7.018 to 149.418°	7.114 to 149.836°
Reflections collected	11498	17352
Independent reflections	2436	2487
R(int)	0.0511	0.0490
Data / restraints / parameters	2436/0/168	2487/0/219
Goof (F ²)	1.157	1.058
R ₁ [I>2σ(I)]	0.0440	0.0398
wR ₂ [all data]	0.1271	0.0964
Max/min res. e density [eÅ ⁻³]	0.23 and -0.22	0.25 and -0.20

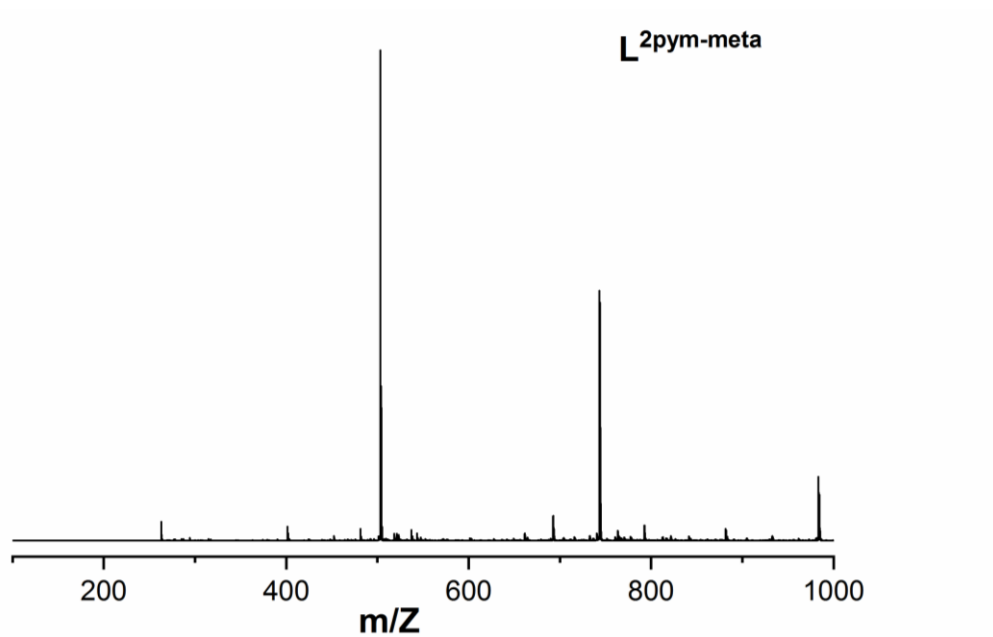


Figure S44. Mass spectrum of $L^{2pym-meta}$.

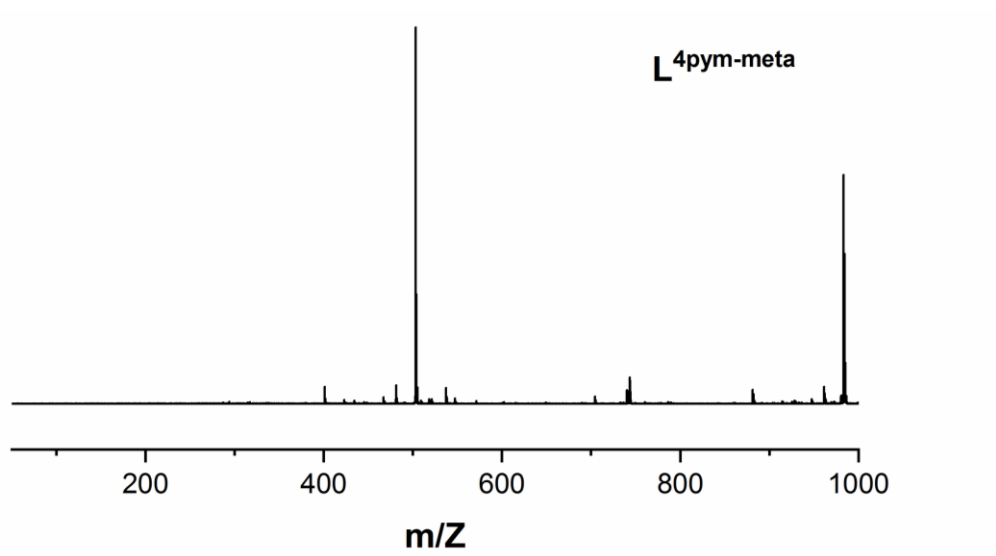


Figure S46. Mass spectrum of $L^{4pym-meta}$.

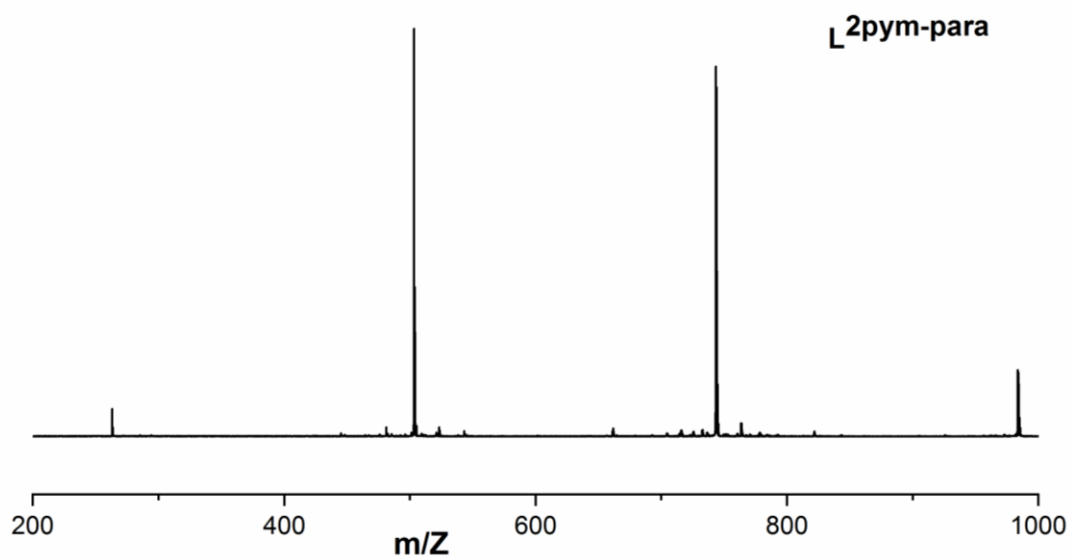


Figure S47. Mass spectrum of L₂pym-para.

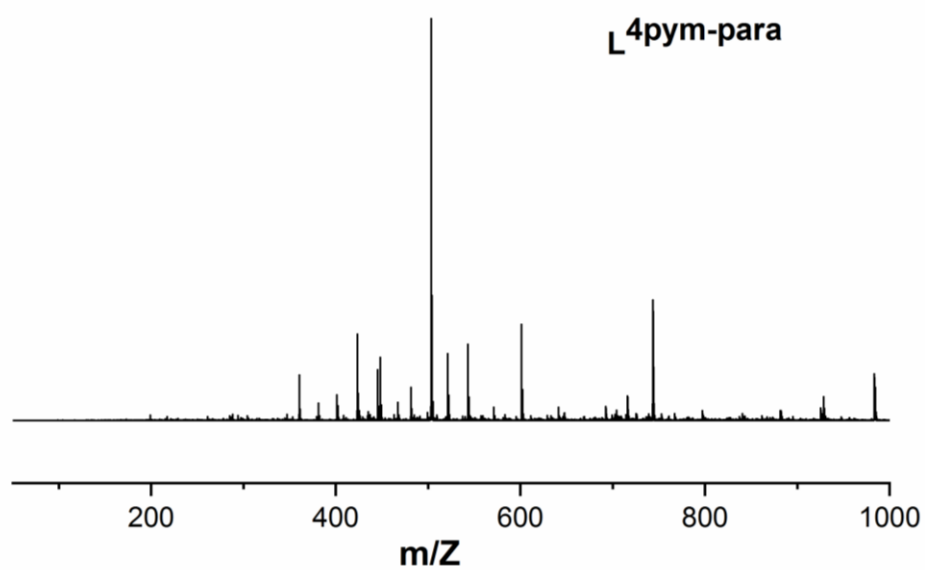


Figure S48. Mass spectrum of L₄pym-para.

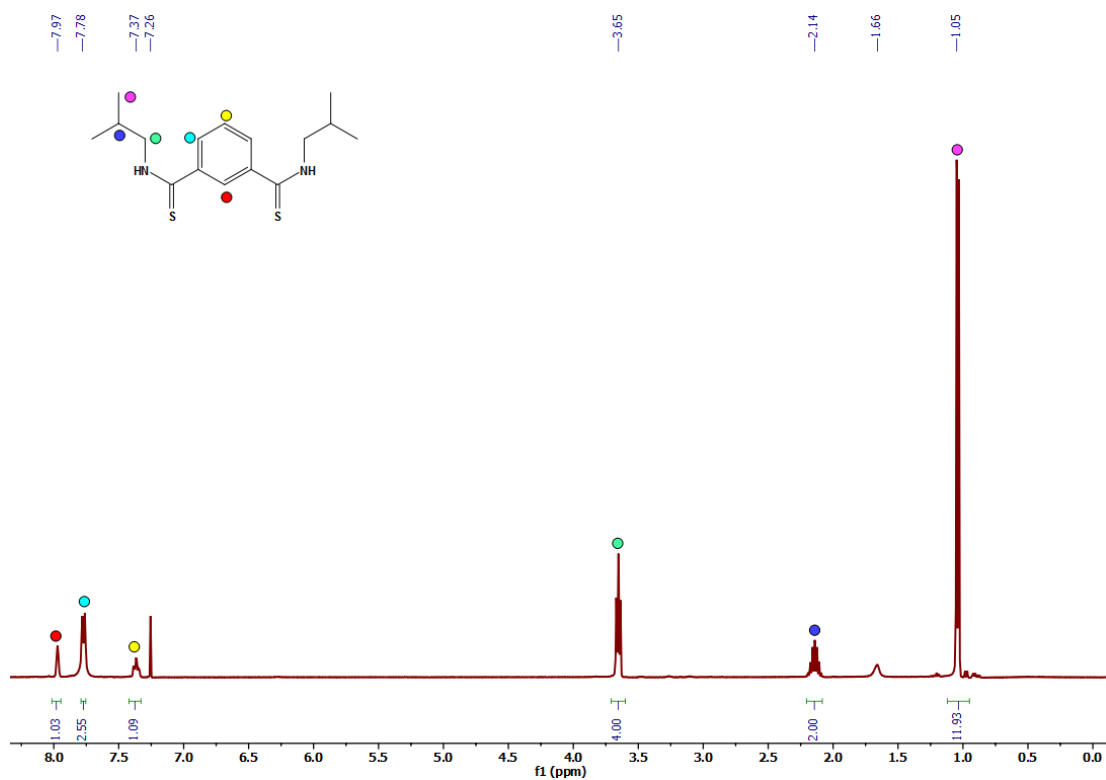


Figure S49. ¹H NMR spectrum (400MHz) of N¹,N⁴-diisobutylbenzene-1,3-bis(carbothioamide) in CDCl₃.

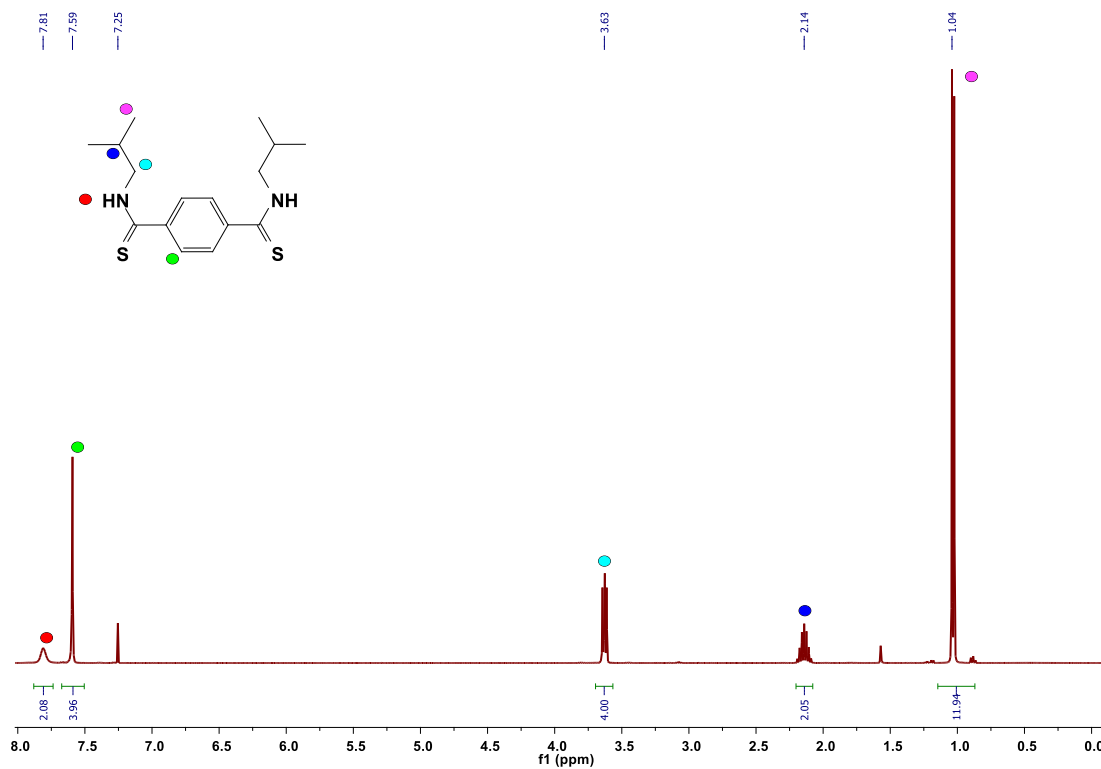


Figure S50. ¹H NMR spectrum (400 MHz) of N¹,N⁴-diisobutylbenzene-1,4-bis(carbothioamide) in CDCl₃.

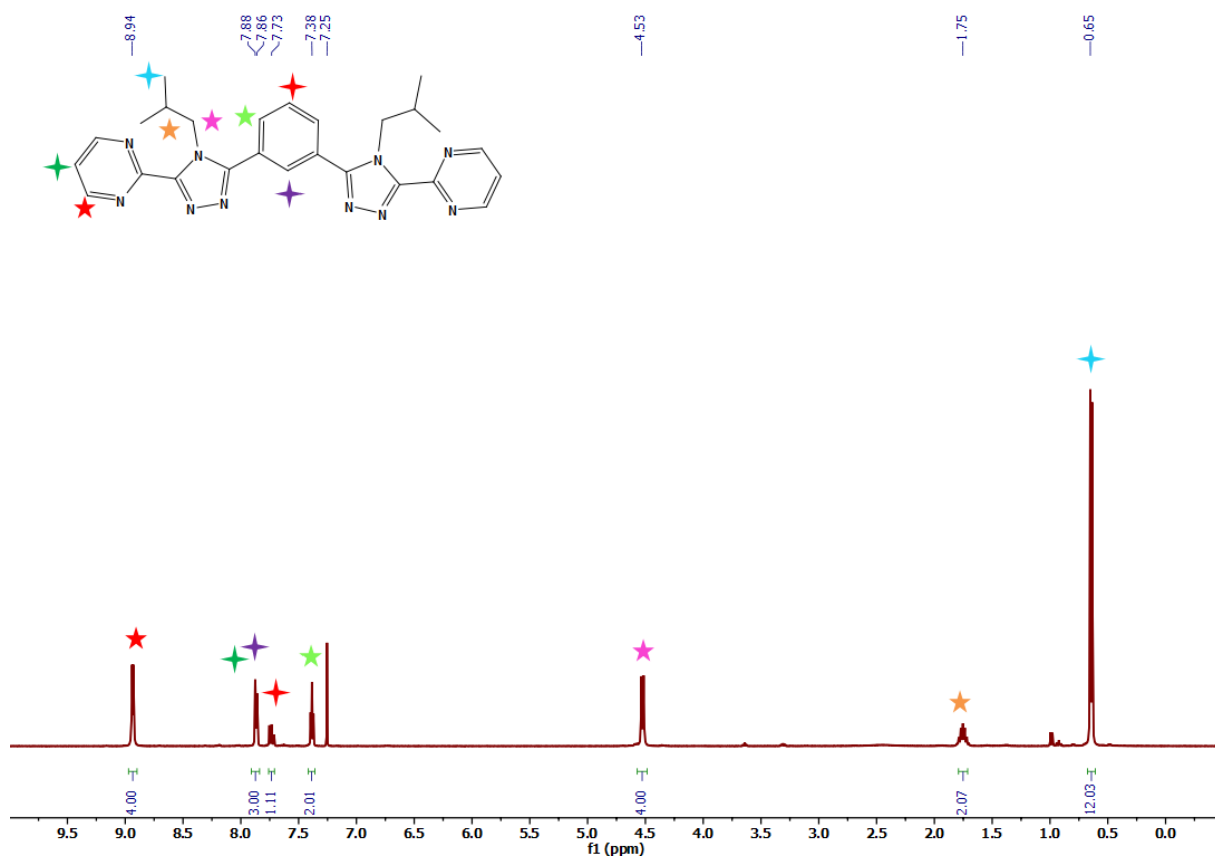


Figure S51. ^1H NMR spectrum (400 MHz) of 1,3-bis(4-isobutyl-5-(pyrimidin-2-yl)-4H-1,2,4-triazol-3-yl)benzene ($\text{L}^2\text{pym-meta}$) in CDCl_3 .

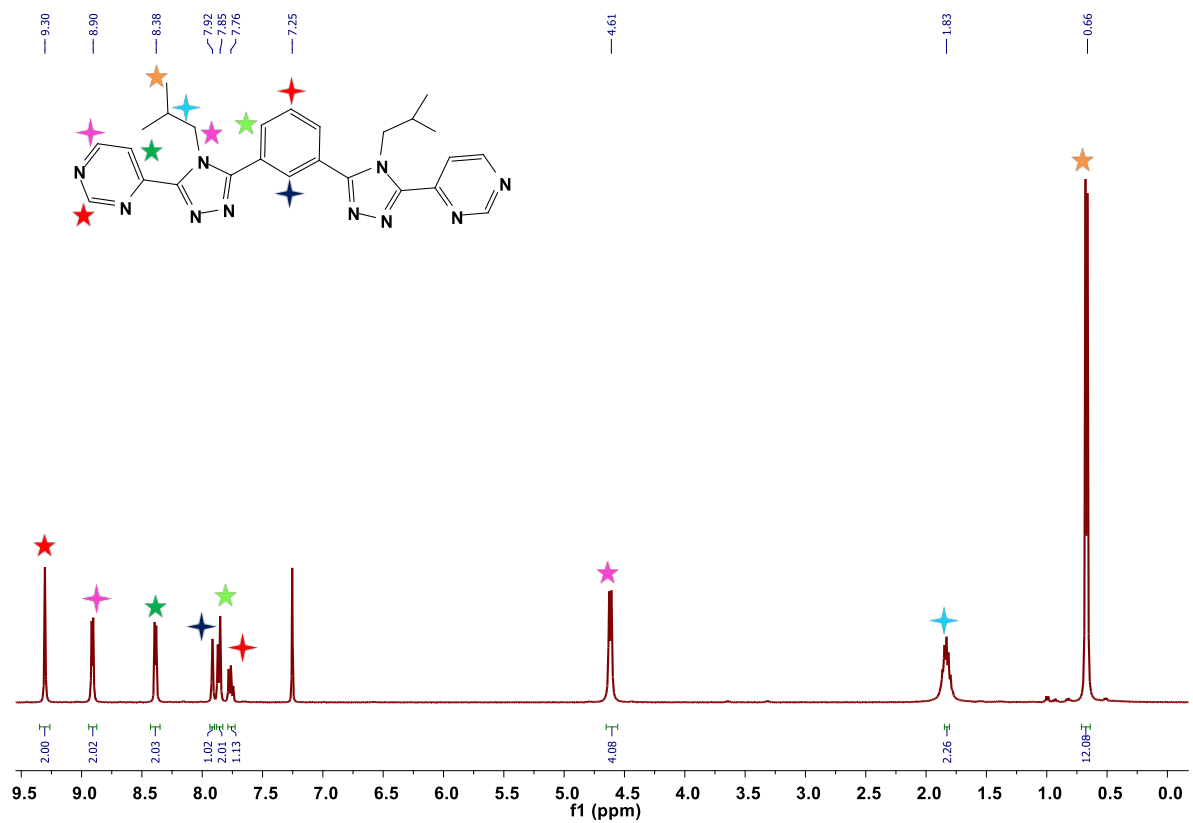


Figure S52. ¹H NMR spectrum (400 MHz) of 1,3-bis(4-isobutyl-5-(pyrimidin-4-yl)-4H-1,2,4-triazol-3-yl)benzene (**L⁴pym-meta**) in CDCl₃.

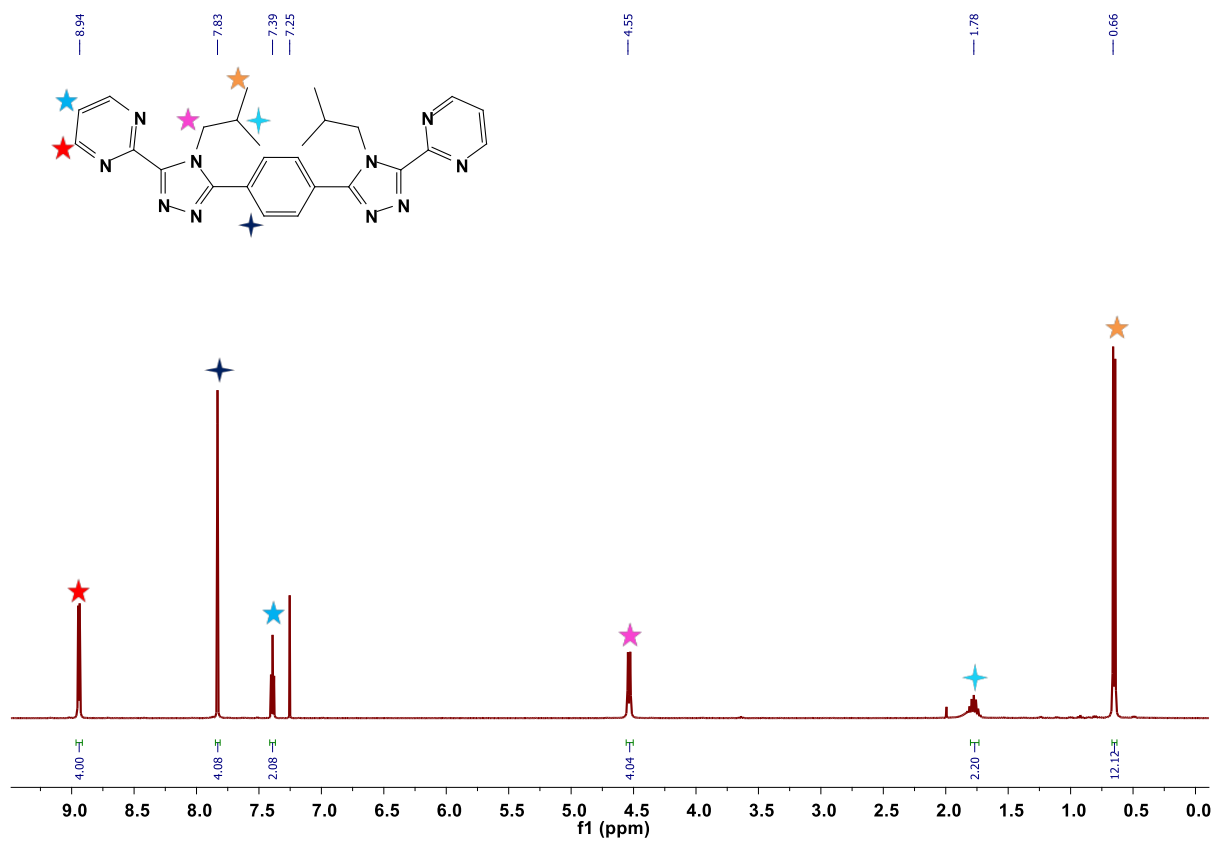


Figure S53. ¹H NMR spectrum (400 MHz) of 1,4-bis(4-isobutyl-5-(pyrimidin-2-yl)-4H-1,2,4-triazol-3-yl)benzene (**L²pym-para**) in CDCl₃.

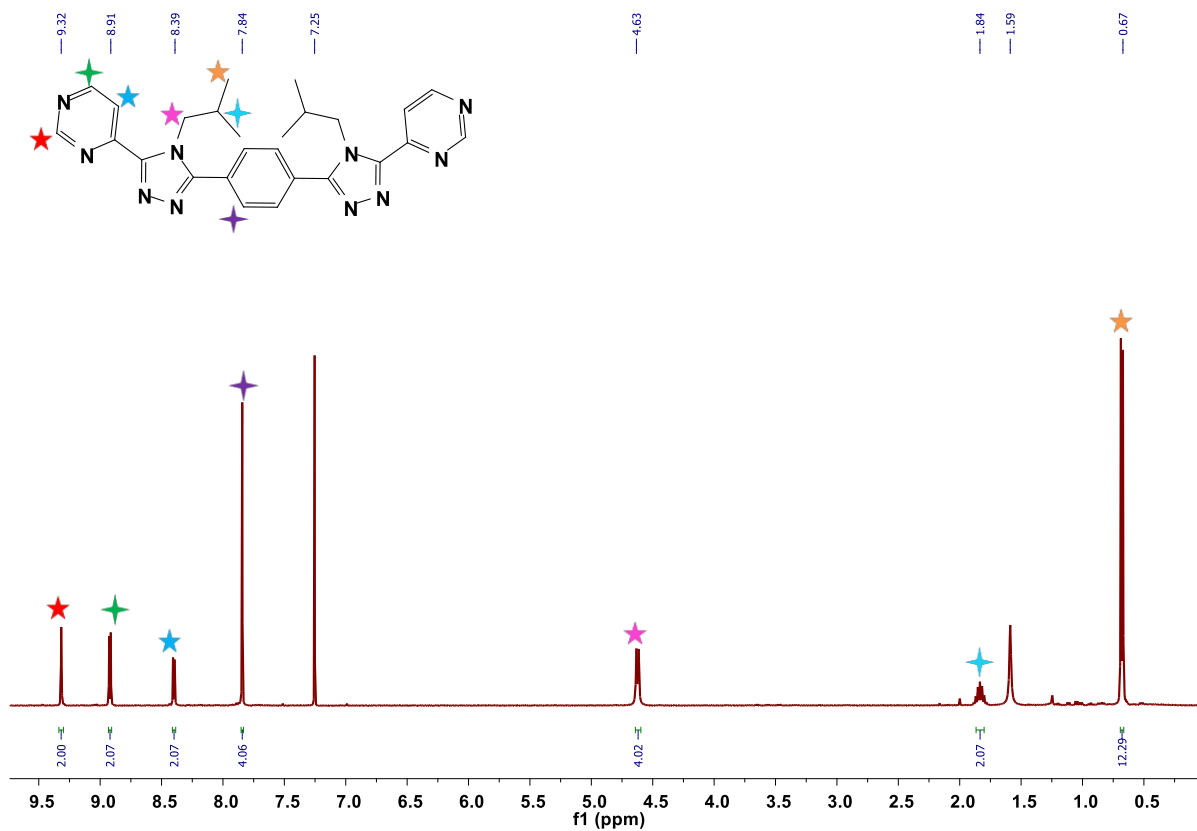


Figure S54. 1H NMR spectrum (400 MHz) of 1,4-bis(4-isobutyl-5-(pyrimidin-4-yl)-4H-1,2,4-triazol-3-yl)benzene ($L^{4pym-para}$) in $CDCl_3$.

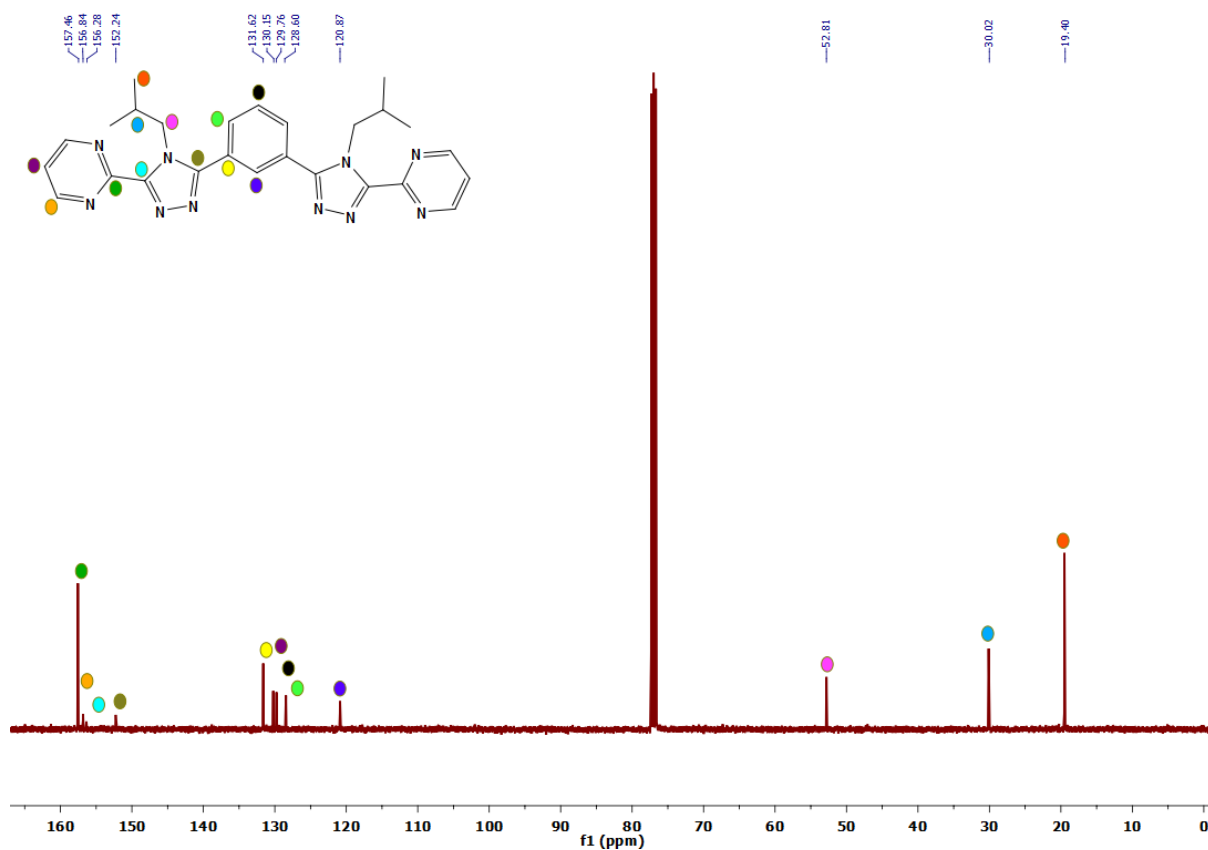


Figure S55. ¹³C NMR spectrum (400 MHz) of 1,3-bis(4-isobutyl-5-(pyrimidin-2-yl)-4H-1,2,4-triazol-3-yl)benzene (**L²pym-meta**) in CDCl₃.

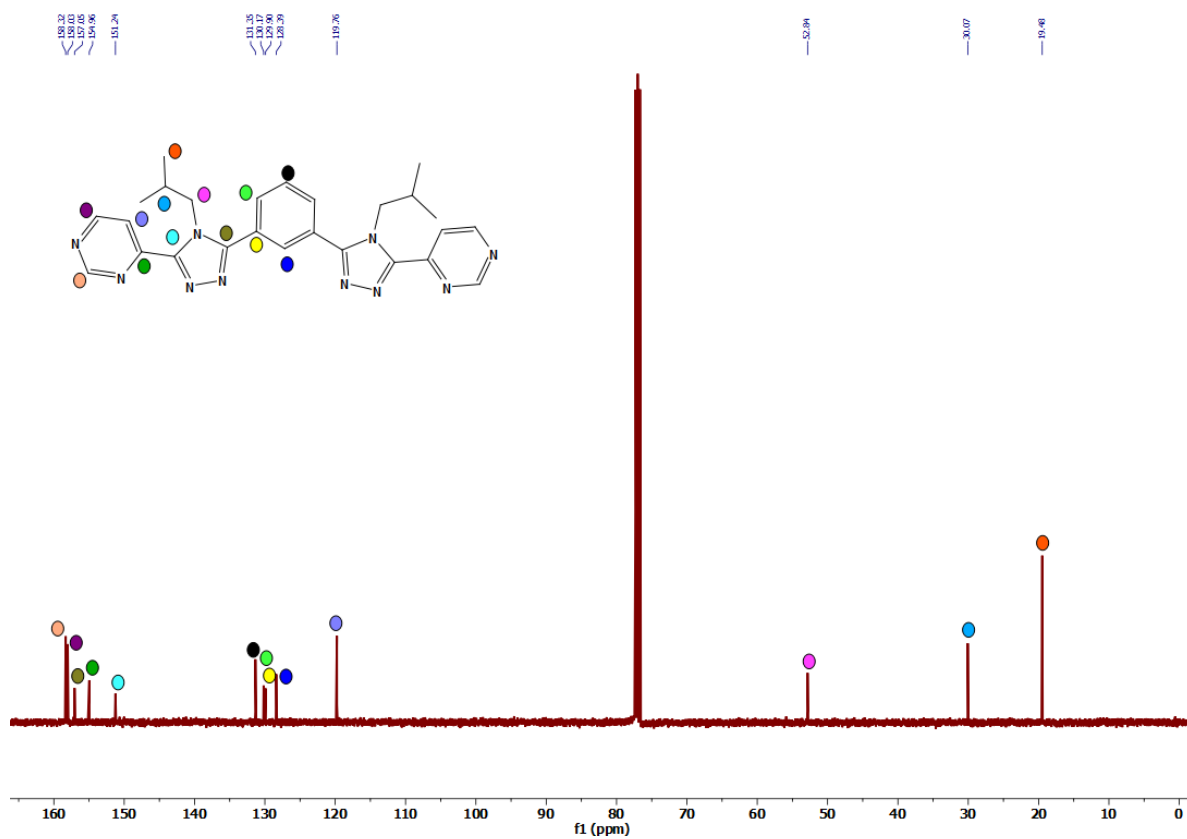


Figure S56. ^{13}C NMR spectrum (400 MHz) of 1,3-bis(4-isobutyl-5-(pyrimidin-4-yl)-4H-1,2,4-triazol-3-yl)benzene ($\text{L}^4\text{pym-meta}$) in CDCl_3 .

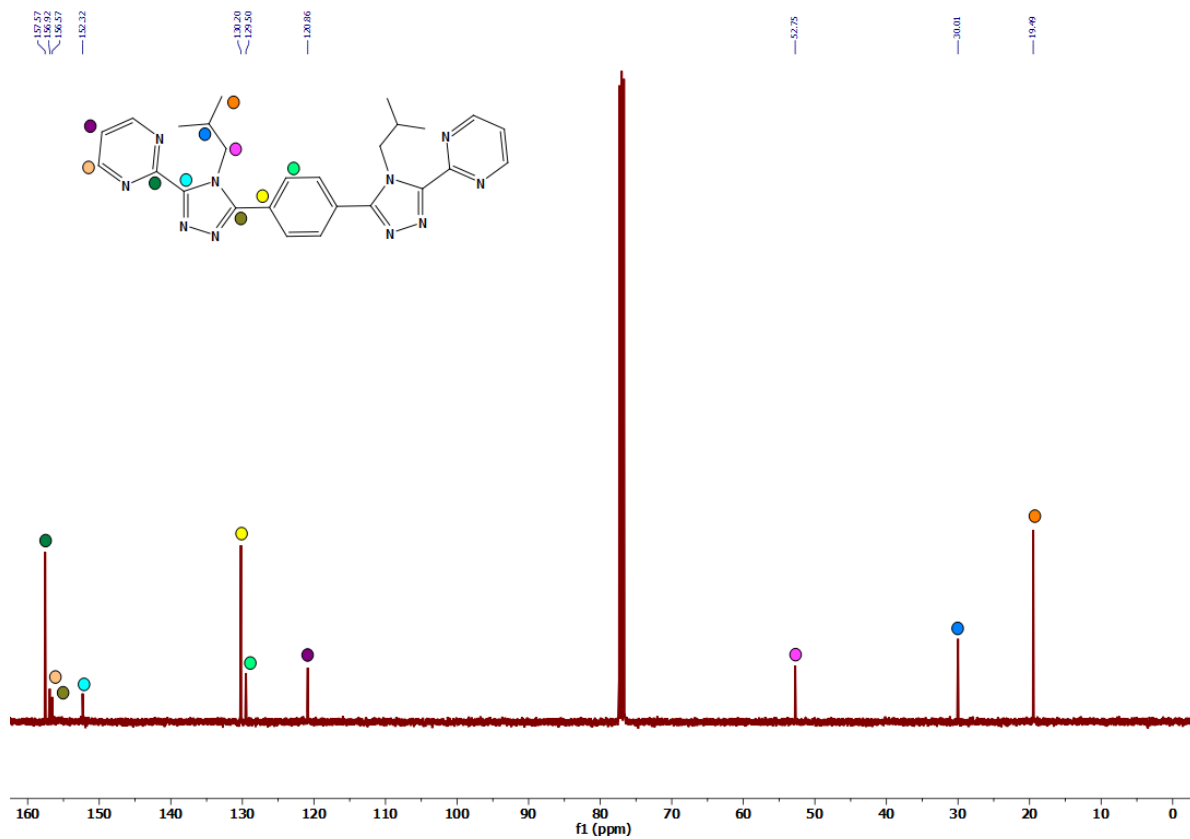


Figure S57. ^{13}C NMR spectrum (400 MHz) of 1,4-bis(4-isobutyl-5-(pyrimidin-2-yl)-4H-1,2,4-triazol-3-yl)benzene ($\text{L}^2\text{pym-para}$) in CDCl_3 .

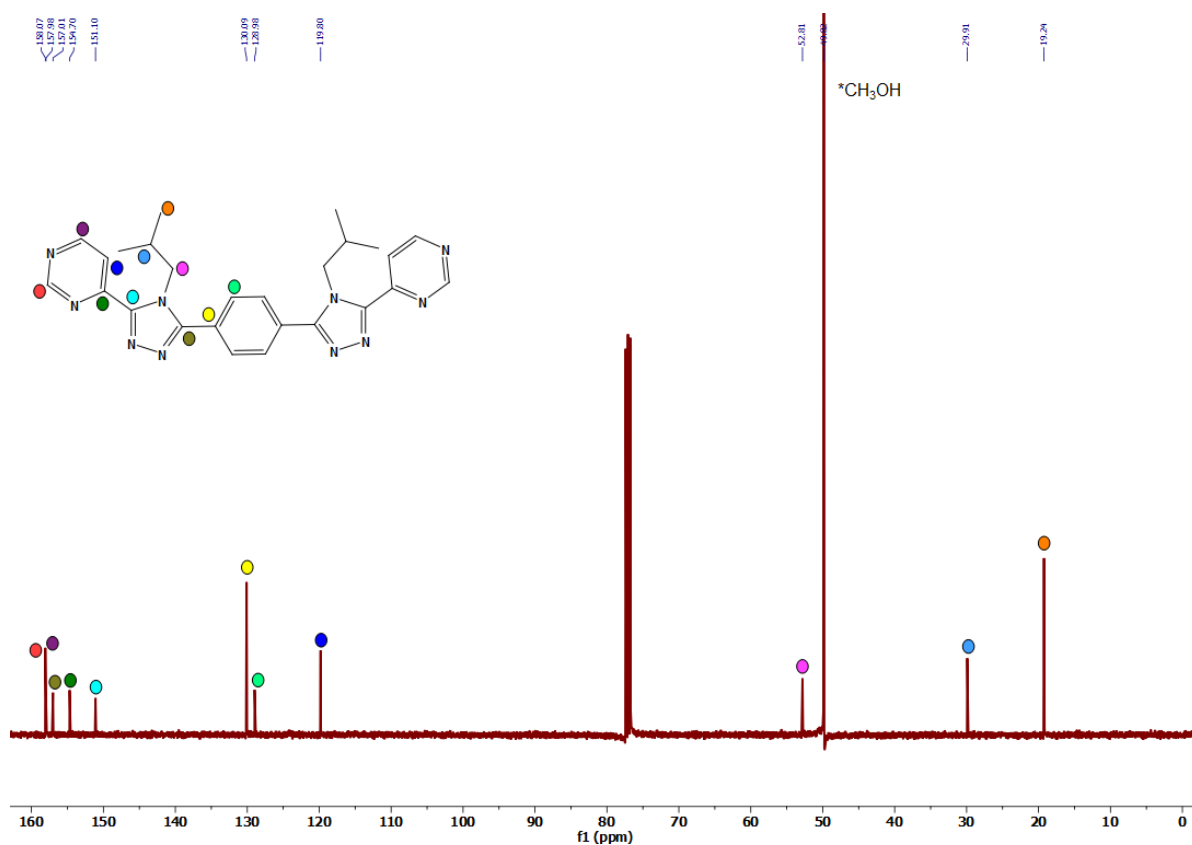


Figure S58. ¹³C NMR spectrum (400 MHz) of 1,4-bis(4-isobutyl-5-(pyrimidin-4-yl)-4H-1,2,4-triazol-3-yl)benzene (**L⁴pym-para**) in CDCl₃.

References

1. P. van der Sluis and A. L. Spek, *Acta Crystallogr., Sect. A: Found. Crystallogr.*, 1990, **A46**, 194-201.
2. A. Spek, *J. Appl. Crystallogr.*, 2003, **36**, 7-13.
3. C. F. Macrae, I. J. Bruno, J. A. Chisolm, P. R. Edgington, P. McCabe, E. Pidcock, L. Rodriguez-Monge, R. Taylor, J. van de Streek and P. A. Wood, *J. Appl. Cryst.*, 2008, **41**, 466-470.
4. *POVray Persistence of Vision Raytracer*, Persistence of Vision Pty. Ltd., 2013.